Nanometrology
FY 2004/2005 Projects

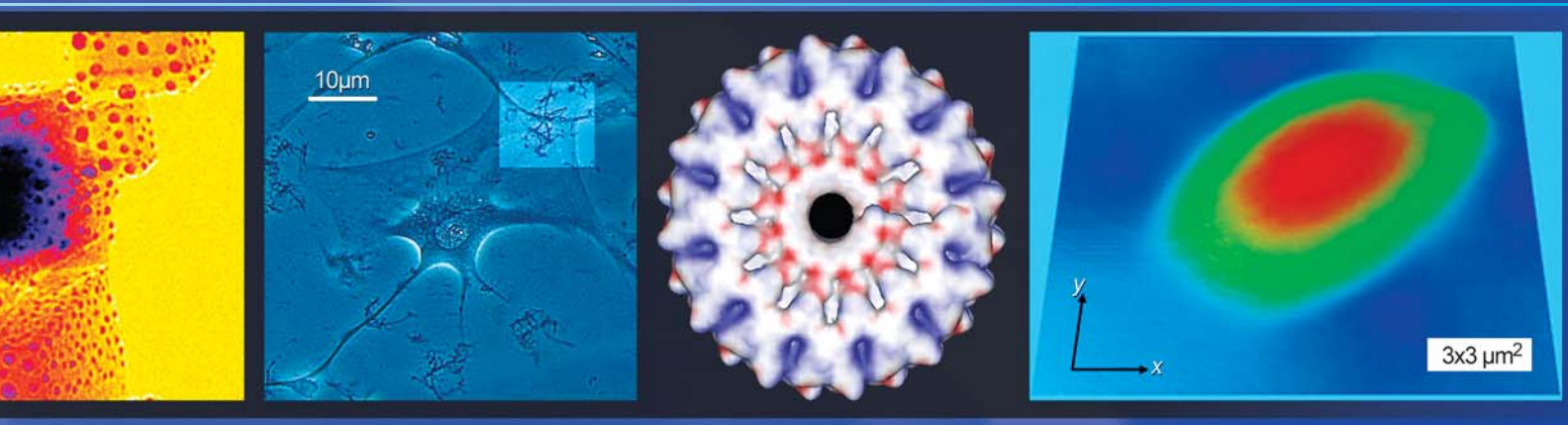

MSEL
Materials Science and Engineering Laboratory

NIST
National Institute of Standards and Technology
Technology Administration
U.S. Department of Commerce

NISTIR 7130

April 2005

On the Cover:

Left to Right:

Fig. 1 – Nanoscale Characterization by Electron Microscopy—MgO cubes with surfaces decorated by small gold particles. These particle ensembles are used in model studies of 3D chemical imaging at the nanoscale (electron tomography).

Fig. 2 – Carbon Nanotubes—Vascular smooth muscle cell growing on a cluster of multiwalled carbon nanotubes on a glass substrate.

Fig. 3 – Wet Nanomanufacturing—Molecular model of the artificial membrane pore viewed from top.

Fig. 4 – Friction Scaling—3D profile, obtained using the replica technique, of the tips used in the friction measurements.

National Institute of Standards and Technology
Hratch G. Semerjian
Acting Director

Technology Administration
Phillip J. Bond
Undersecretary of
Commerce for Technology

U.S. Department of Commerce
Carlos M. Gutierrez
Secretary

Materials Science and Engineering Laboratory

Nanometrology FY 2004/2005 Projects

MSEL

Clare Allocca
Senior Scientific Advisor to the Director, MSEL

Stephen Freiman
Deputy Director, MSEL

NISTIR 7130

April 2005

Table of Contents

Nanofabrication and Processing

Executive Summary

The burgeoning field of nanomaterials extends across the full range of traditional material classes, including all forms of metals, polymers, and ceramics. No previous materials technology has shown concurrent advances in research and industry as does the field of nanomaterials in mechanical devices, electronic, magnetic, and optical components, quantum computing, biotechnology, and as-yet unanticipated exploitations of as-yet undiscovered novel properties of assemblies. There is growing excitement surrounding the ability of some molecules or particles to self-assemble at the nanoscale to form new materials with unusual properties. Nanometrology, *i.e.*, the ability to conduct measurements at these dimensions, to characterize the materials, and to elucidate the structure and nature of these new and novel assemblies, is a requisite and fundamental cornerstone that must be established securely if this technology is to flourish.

NIST is uniquely positioned to lead the development of the measurement methods, instrumentation, standards, and reference materials that together will form the metrological infrastructure essential to the success of nanotechnology.

The MSEL Nanometrology Program incorporates basic measurement metrologies to determine material properties, process monitoring at the nanoscale, nanomanufacturing and fabrication techniques, and structural characterization and analysis techniques such as advanced imaging and multiscale modeling. The Program comprises projects in the Ceramics, Materials Reliability, Metallurgy, and Polymers Divisions, and includes structural characterization using neutron scattering at the NIST Center for Neutron Research (NCNR). The projects cover a wide range of measurement and characterization methods grouped into the areas of mechanical property measurement, chemical and structural characterization and imaging, fabrication and monitoring of nanoprocesses and events, and modeling of nanoscale properties. In each area, we work to advance basic measurement capabilities and lead the intercomparison, standardization, and calibration of test methods. The newly completed Advanced Measurement Laboratory at the NIST Gaithersburg site provides an incomparable environment for accurate nanoscale metrology.

In the area of nanomechanics, we are developing and standardizing techniques for determining nanoscale elastic properties (elastic moduli, Poisson's ratio, and internal stress), plastic deformation, density, adhesion, friction, stiction, and tribological behavior. Work in nanoindentation, used extensively in determining mechanical properties of thin films and nanostructures, focuses on developing traceable calibration methodologies and standard test methods. We also use atomic force acoustic microscopy, surface acoustic wave spectroscopy, and Brillouin light scattering to measure the mechanical properties of thin films. In addition, we are developing micro- and nano-scale structures and test methods to measure strength and fracture behavior of interfaces and materials having very small volumes. Experimental studies are accompanied by efforts in the theory, modeling, and prediction of material properties and behavior extending from nanoscale to macroscale dimensions. Modeling efforts include large-scale finite element methods, multiscale Green's-function methods, classical atomistic simulations, and first principles, quantum mechanical calculations using density functional theory.

Nanocharacterization utilizes neutron and x-ray beam lines at three facilities: the NCNR; the National Synchrotron Light Source at Brookhaven National Laboratory; and the Advanced Photon Source at Argonne National Laboratory. Innovative scattering and spectroscopy methods are advancing our ability to obtain a wide range of chemical and structural information at the nanoscale, including chemical bond identification and orientation, polyelectrolyte dynamics, and equilibrium structures. In collaboration with three other NIST laboratories, we are developing electron microscopy and spectroscopy instrumentation for quantitative, 3D chemical imaging at the nanoscale. Other characterization projects include work on gradient reference specimens for the calibration of advanced scanning probe microscopy, and the application of carbon nanotubes as physical probes of cell membranes.

Efforts in the nanofabrication and processing include the study of electrochemical and microfluidic methods for fabricating nanostructures, novel approaches to nanocalorimetry for the study of interfacial reactions, and *in situ* observations of nanoparticle and nanotube dispersion and alignment. A second joint NASA–NIST Workshop was held in order to establish the measurement needs for determination of purity and dispersion of single-wall carbon nanotubes. The results of this workshop will be captured in "NIST Recommended Practice Guides."

Quantitative Nanomechanical Properties

We are developing AFM-based metrology for rapid, nondestructive measurement of mechanical properties with true nanoscale spatial resolution. Atomic force acoustic microscopy methods enable elastic-modulus measurements at either a single point or as a map of local property variations. Complementary information obtained with scanning electron microscopy provides insight into structure-property relations and helps to interpret nanoscale contact-mechanics behavior. The information obtained furthers our understanding of the nanomechanical properties of surfaces, thin films, and nanoscale structures.

Donna C. Hurley

New measurement solutions are required to address the rapidly burgeoning field of nanotechnology. In particular, information about mechanical properties on the nanoscale is needed. Knowledge of properties like elastic modulus and interfacial quality (defects, strain, adhesion, etc.) is critical to successful development of new films and nanoscale assemblies. Such information could also assess integrity or reliability in applications from microelectronics to biotechnology. Existing methods for mechanical-property measurements have drawbacks: they are destructive, limited to specialized test specimens, or not quantitative. Instrumented or "nano-" indentation (NI), a current industry workhorse, will have limited value as scales shrink well below 1 μm, and softer materials are more frequently used.

To meet this need, we are developing tools that exploit the spatial resolution of atomic force microscopy (AFM). Our approach, called atomic force acoustic microscopy (AFAM), involves the vibrational resonance of an AFM cantilever when its tip is in contact with a sample. By comparing the cantilever's contact-resonance frequencies for an unknown material to those for a reference sample with known properties, the indentation modulus M of the unknown material can be determined. [For an isotropic material $M = E/(1-\nu^2)$, where E is Young's modulus and ν is Poisson's ratio.] The small tip radius (~5–50 nm) means that we can obtain *in-situ* elastic stiffness images with nanoscale spatial resolution.

In FY04, we extended our quantitative AFAM techniques in a variety of ways. In one effort, the effect of film thickness on measurement accuracy was investigated. We measured M for three nickel (Ni) films approximately 50, 200 and 800 nm thick. The values of M ranged from 220 GPa to 223 GPa, significantly lower than that expected for bulk polycrystalline Ni. Scanning electron microscopy (SEM) revealed that the films were nanocrystalline (grain diameter < 30 nm). The observed reduction in M may be attributed to an increased volume fraction of grain boundaries in the nanocrystalline films. More importantly, the average values of M for all three films were the same within measurement uncertainty (~10 %). Thus the AFAM results were not influenced by the elastic properties of the silicon substrate, even for a 50 nm film. This behavior is due to the fact that the AFAM stress field extends less than 100 nm into the sample and decreases rapidly with depth due to the small applied static loads (0.3–3 μN) and small radius of contact (5–25 nm). Our result contrasts sharply with nanoindentation, in which substrate properties must be included to accurately measure submicrometer films.

The elastic properties of the 800 nm Ni film were also measured using NI, microtensile testing, and surface acoustic wave spectroscopy (SAWS). Both AFAM and NI measure the film's out-of-plane indentation modulus. The results were in excellent agreement, validating AFAM as a quantitative method in spite of its relative newness. Microtensile testing values for the in-plane Young's modulus of the film were not consistent with the AFAM and NI results if the film was assumed to be elastically isotropic. The apparently contradictory results were reconciled by use of a transversely anisotropic model for the film's elastic properties. This model is consistent with the strong <111> film texture observed by x-ray diffraction. When analyzed with the same model, the SAWS results indicated that the film density was only slightly lower (< 5 %) than the bulk value. These results illustrate a relatively straightforward way to interpret mechanical-property measurements of thin films that is based on a more physically realistic model than the simple assumption of elastic isotropy.

Another effort investigated the effects of relative humidity (RH) on AFAM measurements. AFAM contact

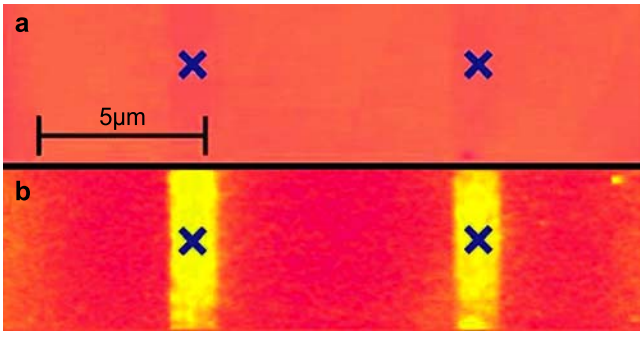

Figure 1: *a) AFM tapping-mode topography and b) AFAM relative-stiffness images of Si with n-octyldimethylchlorosilane SAM.*

stiffness measurements may be affected by a variable water layer between the tip and sample, at least in some cases. By refining our data analysis methods to include the effects of such a layer, apparent correlations between the measured values of *M* and the ambient RH were eliminated. This year we also developed a RH-controlled AFM chamber in order to systematically study these effects. Samples for the experiments were provided by the Polymers Division and consisted of patterned self-assembled monolayers (SAM) of n-octyldimethylchloro-silane on Si substrates. Through controlled ultraviolet-ozone exposure, the relative hydrophobic/hydrophilic nature of the SAM was adjusted in different sample regions. Figure 1 shows an AFM topography image and an AFAM relative-stiffness image for a SAM/Si sample. The SAM stripes are virtually invisible in the topography image, even at very high resolution (10 nm full scale height). However, the AFAM image clearly reveals the hydrophobic SAM stripes. The regions covered by the SAM appear more compliant (lower contact stiffness) due to AFAM's sensitivity to local variations in the tip-sample adhesion. We are currently performing further experiments on similar samples in order to quantify how humidity and adhesion effects can be distinguished from true mechanical-property variations.

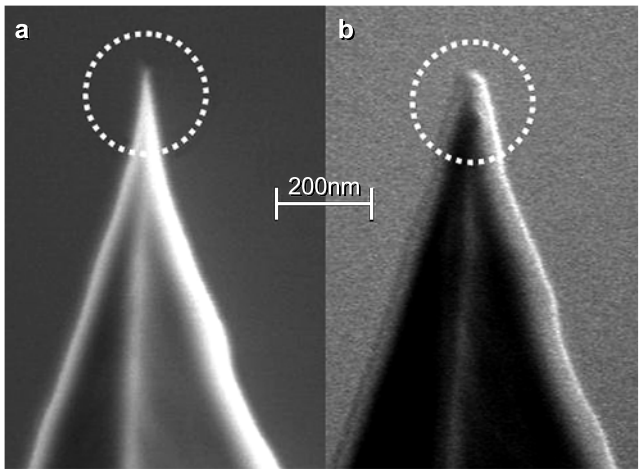

Figure 2: *SEM images of AFM cantilever tip a) before use and b) after repeated AFAM contact experiments. The circled regions indicate the tip wear that occurred through use.*

AFAM contact-resonance frequencies depend not only on elastic properties, but also on the value of the tip radius *R*. Thus knowledge of *R* and how it changes over time is essential for accurate measurements of elastic properties. To address this issue, we performed AFAM experiments with different AFM cantilevers on a sample with known elastic properties. The first measurements were done at relatively low static loads; the load was then successively increased up to several micronewtons to try to break and/or plastically deform the tip. High-magnification SEM images were obtained before and after each AFAM measurement. As can be seen in Figure 2, *R* increased with use, indicating tip wear. Values of *R* measured from the SEM images were compared to the values obtained from AFAM data using a Hertzian contact-mechanics model. The AFAM values of *R* were consistently smaller than the SEM values. Further data analysis and additional experiments are planned to clarify this issue. The knowledge gained in this way will help us to refine our understanding of AFAM contact mechanics, beyond the Hertz approximation, in order to improve measurement accuracy and repeatability.

In related work, we are performing finite-element studies of the AFM cantilever. The finite-element mesh is based on actual cantilever dimensions from SEM images and includes elastic anisotropy. The predicted free-space resonant frequencies are in excellent agreement with those observed experimentally. Work is underway to predict the vibrational behavior in contact. These results will allow us to refine our data analysis models and thus improve measurement accuracy.

The research described above involves either *quantitative single-point* measurements, or *qualitative imaging* of relative stiffness. In FY04, we worked to realize our ultimate goal of *quantitative nanomechanical mapping*. Critical to our success is a new frequency tracking circuit that can determine the contact-resonance frequencies at each image pixel. The circuit is based on digital signal processing architecture that enables rapid data acquisition (typically < 30 min. for a 256 × 256 image). We have begun to obtain resonance-frequency images for a variety of materials. Recent enhancements to our AFM mean that we can acquire images from not only the flexural modes, but also the torsional modes of the cantilever. By combining information from flexural and torsional images, it may be possible to determine simultaneously both Young's modulus and Poisson's ratio for an isotropic material. Work in upcoming months will focus on issues related to quantitative image interpretation such as calibration procedures, cantilever selection, tip wear, and choice of contact-mechanics model. Each of these elements plays a role in attaining our goal of truly quantitative nanomechanical imaging.

For More Information on this Topic

D.C. Hurley (Materials Reliability Division, NIST)

Mechanical Metrology for Small-Scale Structures

Myriad industrial and biological systems are composed of small-scale structures for which the mechanical behavior is not accurately known. Optimizing the performance and reliability of these systems requires either mechanical property measurements on specimens of these structures harvested from the appropriate phases or interfaces of the system, or the ability to test these structures in situ. *We are developing standardized testing configurations and methodologies for localized measurements of strength and fracture toughness of materials and interfaces at the micro- to nanometer-length scale.*

Edwin R. Fuller, Jr. and George D. Quinn

This project aims to: (1) measure mechanical properties of microstructures for myriad industrial and biological systems that cannot be fabricated in bulk samples; (2) study small-scale phenomena that may be controlled by surface effects, *e.g.*, the influence of surface stresses on crack nucleation and extension; and (3) obtain quantitative mechanical property data of materials and interfaces for designing small-scale structures and components and for assessing their mechanical reliability. To address these goals, well-characterized testing configurations must be developed for small-scale measurements of strength and crack extension. We are pursuing four tasks: (1) configuration design and finite element analysis; (2) specimen fabrication; (3) mechanical testing and fracture analysis (fractography); and (4) length and force metrology. Work in the Ceramics Division this year has focused on the first and third areas. Two collaborations were established in the fabrication task: one with James A. Beall of the Quantum Electrical Metrology Division (817) in NIST Boulder, and one with Northwestern University. Work in the fourth task will come in subsequent years, most likely in collaboration with the Manufacturing Engineering Laboratory. Significant progress has been made in the design of a compressively loaded test configuration with a well-defined, tensile gage section. Such a specimen can be loaded using a depth-sensing nanoindenter as a universal testing machine, thereby giving a record of both applied load and load-point displacement. One of these specimens, fabricated by James Beall from a silicon wafer by deep reactive ion etching, is shown in the right-side of Figure 1. The configuration is similar to a theta specimen, except that the geometry is hexagonal. When a load (per unit thickness) is applied to the top beam, a uniform uniaxial tensile stress results in the middle gage section. Finite element analysis gives (horizontal) gage section stresses on the order of 1.25 GPa for 50 mN/μm of applied load. For a 2 N applied load, these 100 mm-thick specimens generate 500 MPa of tensile stress in the gage section. The left-side of Figure 1 shows a reconstructed failed specimen. The insert shows the fracture surface of the gage section, and the two [111] cleavage facets that were formed. Alternate geometries, including a round theta specimen, are also being considered.

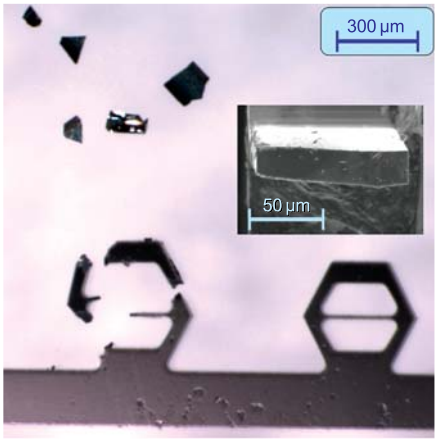

Figure 1: *Prototype specimen design.*

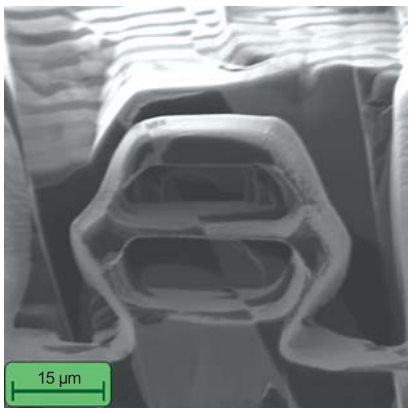

Figure 2: *Hexagonal theta specimen by FIBing.*

To extend this technique to a wide variety of materials and systems, general fabrication procedures need to be developed. Towards this objective, focused-ion-beam (FIB) milling is being explored in collaboration with Northwestern University. Figure 2 shows our first attempt at producing a hexagonal theta specimen by FIBing. It has been scaled-down by about a factor of 10, and is fabricated from a lamellar directionally solidified eutectic of $Ni_{0.5}Co_{0.5}O$ and ZrO_2.

Contributors and Collaborators

D. Xiang, D.T. Smith (Ceramics Division, NIST); A. Jillavenkatesa (Standards Services Division, NIST); J.A. Beall (Quantum Electrical Metrology Division, NIST); N. Alem, V.P. Dravid (Northwestern University)

Nanoindentation Methods and Standards

Nanoindentation has rapidly become the method of choice for quantitative determination of mechanical properties of thin films and small volumes of material, but standardization efforts have lagged far behind the application of the technique in industrial research and development. Over 1000 commercial nanoindentation instruments from a variety of manufacturers are currently in use, with no traceable force calibration and an extremely limited choice of standardized test methods. We work with standards groups and National Measurement Institutes around the world to develop standard reference materials (SRMs), traceable calibration transducers, and robust, reliable methods for obtaining and analyzing nanoindentation data, so that nanoindentation results can be used with confidence in product design and specification.

Douglas T. Smith

Nanoindentation is the most commonly used method for determining hardness and elastic properties of small volumes of materials. In this technique, a diamond indenter is pushed into a specimen surface, and the force on and displacement into the surface are recorded. The technique is capable of providing information on the elastic and plastic deformation of a specimen for indentations as shallow as 5 nm to 10 nm, and requires minimal specimen preparation effort. It is routinely used to measure the mechanical properties of thin films. However, there are only a very limited number of accepted test methods available, and no means to traceably calibrate or verify the performance of nanoindentation instruments. This leads to large interlaboratory variations in results, particularly for hard, high modulus materials, and prevents the use of nanoindentation in thin film or coating product specifications.

In many mechanical test methods, including nanoindentation, a force is applied to a specimen, and some displacement is measured. Traceable displacement measurement by interferometry is well established. Force measurement is more problematic, however, because the SI unit for force is still based on an artifact kilogram mass. The Microforce Competence Program at NIST has developed a primary realization of force, traceable to electronic and length SI units, for force calibration in the range 1 mN to 10 nN. As part of this program, transfer force cells are being developed that will allow force calibration, traceable to NIST, for commercial nanomechanical test equipment such as nanoindentation machines and atomic force microscopes. One such transfer force cell was calibrated against the NIST primary force balance to an uncertainty less than 0.5 % for forces in the range 0.05 mN to 5.0 mN. That cell was then mounted, as if it were a specimen, in a popular commercial nanoindentation instrument that had been recently calibrated by its manufacturer using their recommended force calibration procedure. The figure shows the error in the nanoindentation force recorded by the instrument, relative to the traceable force cell reading. For forces above 2 mN, the recorded force is within the 1 % uncertainty required by most draft standards for nanoindentation machines. However, for lower applied force, the error increases dramatically, and at 0.05 mN, the recorded force is almost 18 % below the actual applied force.

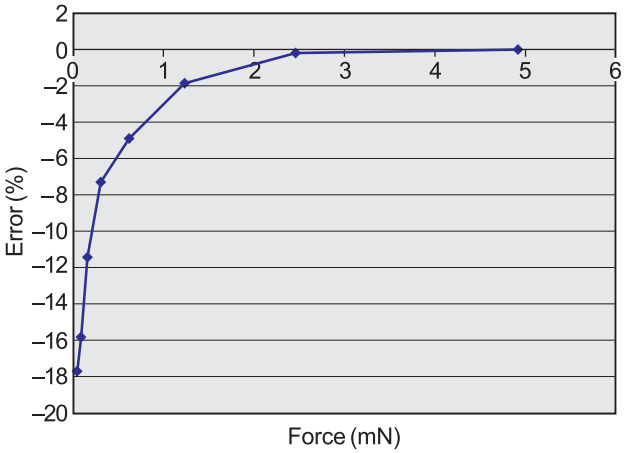

Figure 1: *The error in the force applied to a specimen by a commercial nanoindentation instrument, as referenced to a traceably calibrated NIST force cell.*

We are also working with both ASTM (E28.06.11) and ISO (TC 164/SC 3) on a wide range of standard test methods for nanoindentation, and an ISO document for the one method has now been approved (ISO 14577). In addition, the Ceramics and Materials Reliability Divisions at NIST are working with the Bundesanstalt für Materialforschung und–prüfung (BAM) in Germany to develop joint thin film SRMs (CRMs, or Certified Reference Materials, in Europe) for use in nanoindentation machine verification.

Contributors and Collaborators

D. Xiang, B. Hockey, G. Quinn (Ceramics Division, NIST); R. Machado (INMETRO, Brazil); J. Pratt (Manufacturing Engineering Laboratory, NIST); D. Hurley (Materials Reliability Division, NIST); U. Beck (BAM, Germany)

Nanotribology and Surface Properties

Accurate adhesion and friction measurements at the nanoscale are emerging as critical issues in device industries and nanotechnology. Measurements characterizing nanometer-thick molecular assemblies and surface textures to control surface properties and to ensure reliability and durability are also needed. Working with device and magnetic storage industries and other agencies, we have designed and built instruments to meet these needs. These instruments are housed in NIST's new Advanced Measurement Laboratory. The facility features vibration isolation, class 1000 clean room standards, and temperature control.

Stephen M. Hsu

The nanotribology and surface properties project was initiated as a part of the MSEL Nanotechnology Initiative. The project aims to develop measurement capability for adhesion, friction, and surface forces at the nanoscale. We interact extensively with many industries and research centers in the U.S. and around the world to promote advances in measurement science and seek consensus standard harmonization in three areas: nanocontacts, nanolubrication, and surface texturing.

Nanocontacts

Adhesion and friction measurements at nanocontacts require accurate detection of normal and lateral forces at nanonewton levels. Scanning probe microscopes use sensitive cantilevers and laser diodes to detect these forces, but this approach introduces rotation of the tips and crosstalk among the xyz planes. To understand the influence of surface forces, many of which are functions of contact area, attention must be focused on determining the real area of contact.

To resolve some of the instrumental challenges, we have engaged instrument makers, such as Hysitron, Veeco, and others, to solicit their inputs and collaborations. At the same time, we have established our own capability in tip fabrication, cantilever spring constant calibration, and tip characterization. Three new instruments were successfully installed as a result of these collaborations: the NIST–Hysitron multiscale friction tester, the NIST nanoadhesion apparatus, and the first prototype of an interferometer microscope from Veeco. We are continuing to work with our partners to develop next-generation instruments as suggested by the Nanometrology Grand Challenges Workshop (NIST, January 2004).

The overall objective of the nanocontacts activity is to develop the constitutive equation of adhesion and friction including the various components of surface forces. With our new adhesion and nanofriction apparatus, we are quantifying the effects of plowing and electrostatic charge on measurements. We continue to work with our external academic partners (UC Berkeley, UC Davis, and Ohio State U) under the Nanotechnology Extramural Initiative to develop friction measurement *via* three approaches: friction measuring MEMS devices, AFM methods, and ultrahigh vacuum friction measurement. These efforts have been successful, and we have gained considerable understanding of how meniscus forces and electrostatic forces can exert significant effects on nanofriction measurements. A NIST special publication summarizing these findings is under preparation.

Nanolubrication

Molecular assemblies can be organized to impart hydrophobicity, anti-adhesion, and friction control characteristics on device surfaces. Supported by other agencies and the magnetic storage industry, this activity focuses on how to measure the effects of controlled composition and spacing on properties of nanometer-thick films. An ultrahigh vacuum scanning tunneling microscope-atomic force microscope was installed in May 2004 to provide imaging capability at the molecular level. A micro-tribometer was also developed to measure the durability of these films. The synchrotron facility operated by the Division's Characterization Methods Group at Brookhaven National Laboratory continues to be vital in characterizing these complex molecular mixtures.

Surface Texturing

Surface texture increasingly is being considered as a tool to control surface energy, polarity, adhesion, and friction. Supported by other agencies and industries, we are pioneering the use of specific surface features such as dimples, triangles, and ellipses at micro- and nanoscale dimensions to supplement molecular assemblies to control surface properties of surfaces. An international cooperative study under the auspices of International Energy Agency (IEA) is underway.

Contributors and Collaborators

C. Ying, R. Gates, J. Chuang, J. Larson–Basse, L. Ives, D. Fischer (Ceramics Division, NIST); B. Bhushan (Ohio State U.); K. Komoupoulas (UC Berkeley); G. Liu (UC Davis); Y.T. Hsia (Seagate); J. Sengers (U. of Maryland); O. Warren (Hysitron); C. Su (Veeco)

Nanomechanics: Coupling Modeling with Experiments

Knowledge of mechanical behavior is critical when designing for device performance and reliability, even for "non-mechanical" systems. However, nanoscale mechanical behavior (including failure) is inherently difficult to measure accurately, and existing modeling tools are only qualitative at best. We are developing modeling techniques that provide quantitative predictions and are validating these results experimentally.

Lyle E. Levine and Anne M. Chaka (838)

Mechanics at the nanoscale is inherently difficult to model accurately. Finite element modeling (FEM) can effectively capture the elastic behavior of macroscopic structures but includes no accurate failure criteria since this depends upon atomic-scale behavior. Classical atomistic simulations can handle enough atoms (millions to billions) to model such events, but these potentials become inaccurate for large strains and they cannot effectively handle chemistry. Quantum-mechanics-based simulations using density functional theory (DFT) are extremely accurate and handle the chemistry exactly, but such simulations are so CPU intensive that they can handle only a few hundred atoms. A combination of all three modeling techniques is required to accurately model device behavior at the nanoscale.

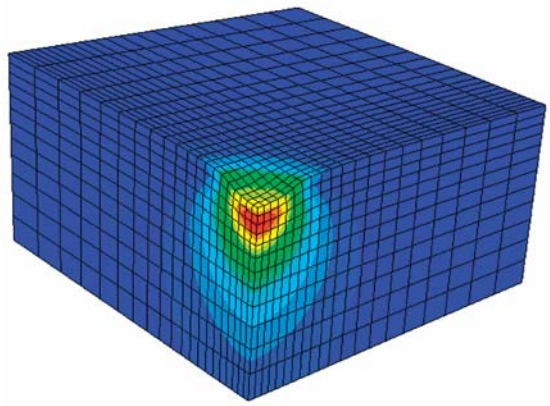

Figure 1: *FEM model of a rigid 100 nm diameter sphere indenting an Al sample to a depth of 10 nm.*

Over the past year, we have developed techniques to handle such multiscale modeling for quasistatic applications. At the macroscale, FEM is used to simulate the elastic behavior of a nanomechanical system. Figure 1 shows an example in which an Al sample is being indented by a rigid 100 nm diameter sphere. The indenter and three of the sample quadrants have been removed to highlight the resulting Von Mises stress distribution after indenting 10 nm. The FEM mesh is fine enough to use the predicted elastic displacement fields to generate boundary conditions and initial atom positions for an atomistic simulation using classical potentials.

The use of classical potentials in a large simulation cell allows the correct propagation of the long-range stresses to the critical regions where bond distortions are large or where chemistry effects need to be explored. In these critical regions, the techniques embed a DFT simulation. Iteratively, the critical region is relaxed using DFT, and the classical cell is relaxed using a Monte-Carlo algorithm. The first application of this hybrid technique was to determine the vacancy formation energy in aluminum as a function of distance (at a fixed angle) away from an edge dislocation. The simulation geometry is shown in Figure 2. The boundary conditions and initial atomic positions were calculated from the known elastic displacement field of an edge dislocation.

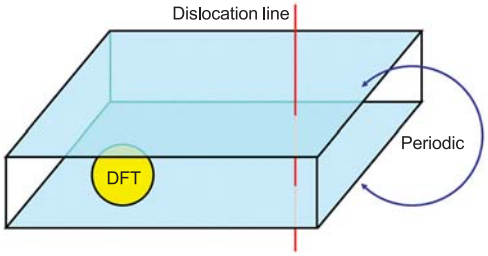

Figure 2: *Diagram of a hybrid simulation for obtaining the vacancy formation energy at different positions relative to an edge dislocation. The large box represents the EAM cell in which the DFT region containing the vacancy was embedded.*

After an initial dislocation nucleation event, nanoindentation progresses through the complex evolution of dislocation structures. For example, the raised lip around the indent is produced by large numbers of dislocations exiting the surface. We are working on modeling the early stages of this process using 3D dislocation dynamics and assuming a random distribution of dislocation sources in the sample.

Finally, connection to experimental measurements requires careful force calibration of the indenter and calibrated atomic force microscopy measurements (AFM) of the indenter tip. These calibrations are mostly complete, and the AFM data will be used to generate a FEM mesh for the simulations. Bulk single-crystal copper samples are being cut and polished using non-contact chemical methods to minimize the dislocation density.

Contributors and Collaborators

S.M. Khan, G. Levi, L. Ma, F. Tavazza (Metallurgy Division, NIST); B. Hockey, R. Machado, D. Smith, R. Wagner, D. Xiang (Ceramics Division, NIST)

Friction Scaling Artifact

Nanofrictional forces are an important factor in the design of nanodevices and assemblies of nanoparticles. Literature data on nanofriction, however, exhibit many discrepancies and have a wide range of scatter. In a series of well-controlled experiments, we have discovered that a significant portion of this discrepancy may actually be attributed to an unintended scratching of the surface by the sharp tips used in making the measurements themselves. Deviation of tip shape from the "ideal" spherical shape is another contributor to the disagreements found among the literature data. This work sheds important insight into the nature of nanoscale friction measurement.

Z. Charles Ying and Stephen M. Hsu

Accurate measurement of nanofriction is emerging as one of the critical issues in nanotechnology. Manipulation of molecules, clusters, and nanoparticles across surfaces to form a functional entity relies on the ability to overcome the resistance of the particles to motion across the surface. Further, reliable operation of micro- and nano-devices often depends on an accurate estimate of lateral loading. Literature data on nanofriction, however, have shown wide ranges of values depending on the length scale of the device. Silicon friction, *e.g.*, shows an order of magnitude variation from 0.03 to 0.25. Such results have led to speculations that there might be an intrinsic scaling effect such that different friction levels would occur across the nano-, micro-, and macro-scales. If proven true, well established friction laws would be invalidated for nanomaterials.

Given the broad technological significance of this issue, we have undertaken a detailed investigation of the nature of this discrepancy. Friction measurements between non-adhering surfaces were carried out in both elastic and plastic deformation regions. Diamond tips of various sizes were used to measure nanofriction forces on well-characterized substrates such as single crystal silicon, silicon dioxide, and calcium fluoride. Experiments were performed using a specially designed multiscale friction tester developed jointly by NIST and Hysitron Incorporated based on a capacitance probe force transducer. In each experiment, the environment was carefully controlled, and the tip penetration into the substrate during sliding was continuously measured.

The size and shape of each tip were characterized using a newly developed "replica technique." Tips were imprinted into a soft material, and the imprints were scanned by AFM and digitally inverted to "reconstruct" the tip in three-dimensional details. Figure 1 shows images of two of the diamond tips used in the experiments. The tip shown in Figure 1(a) is spherical in shape with a 1.2 µm tip radius while Figure 1(b) shows an ellipsoidal shape with nominal radius of 4 µm. The detailed dimensional data are crucial in determining the apparent contact areas and isolating the influence of surface forces.

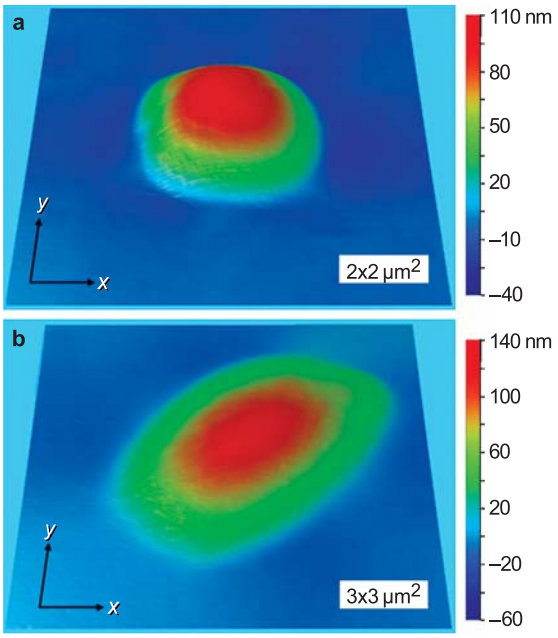

Figure 1: *3D profiles, obtained using the replica technique, of the tips used in the friction measurements.*

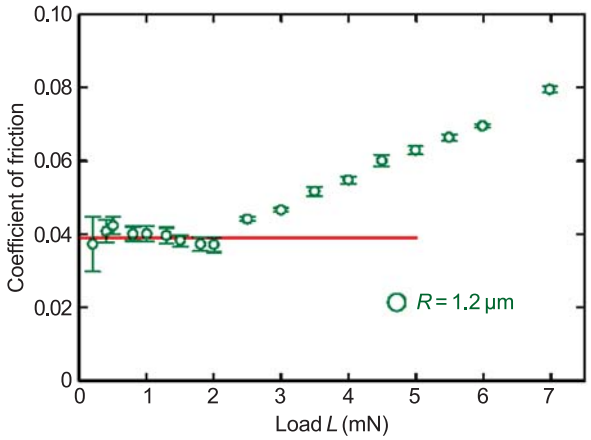

Figure 2: *Coefficient of friction between Si (100) surface and a diamond tip with radius* R = *1.2 µm, as a function of mechanical loading force.*

Figure 2 shows the coefficient of friction (COF) between a Si (100) surface and a diamond tip with tip radius R = 1.2 µm.

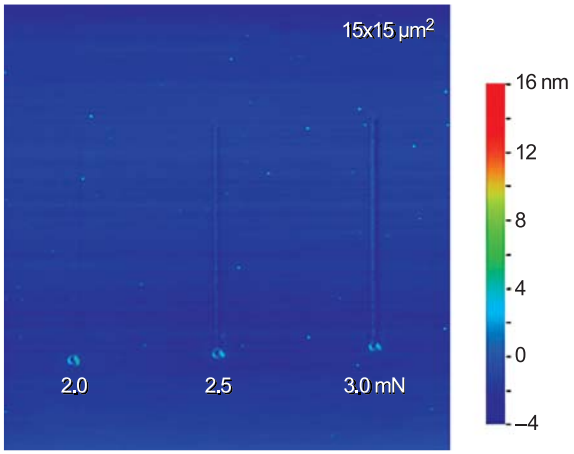

Figure 3: *Image of the silicon surface after friction measurements, showing scratches at 2.5 mN and higher load.*

Two distinct regions can be seen. Initially, the COF is constant up to a load of 2.0 mN. For loads above 2.5 mN, the COF increases with load. This friction transition is contrary to Amoton's law. Subsequent investigation revealed that this change in COF is caused by unintended plowing of the tip into the substrate. Atomic force microscopy, using a sharp tip on the surface, suggests that the COF increase coincides with the first appearance of plastic grooving. In the case of silicon, a groove 5 Å deep and 2000 Å wide was detected on the surface at a load of 2.5 mN (Figure 3).

This observation was repeated for different tips and different substrates. At higher loads, deeper and wider grooves were observed. These results suggested that unintended scratching of the surfaces by the sharp tips used in the friction measurements contributed to the discrepancies among friction data in the literature.

The initiation of plastic grooving can be quantified in terms of contact pressure. By determining the apparent contact area using the digitally inverted tip method, the transition contact pressures could be calculated for all of the observed cases. All the results corresponded to 12 GPa which is approximately the hardness of silicon.

Elastic Plowing

Figure 4 shows the friction data for three tips in the elastic region (no plastic grooving). The data for the two spherical tips with radii $R = 0.5$ µm and 1.2 µm exhibit a common value for the COF. However, a higher friction value was observed for the 4 µm radius tip.

To explain this discrepancy, we tested the various contact mechanics models which require the accurate determination of the real contact areas. Considering a tip plowing through an elastic substrate, the real area of contact is the projected cross-section area of the tip in the direction of sliding. This can be determined from the tip geometry and "penetration depths" across the sliding path. Numerical integration of actual tip size and shape over the sliding path is required. For the hypothesis of "elastic plowing," the calculation shows that the friction force in this regime should be proportional to the projected cross-sectional area in the direction of sliding. Figure 5 confirms this hypothesis for all three tips.

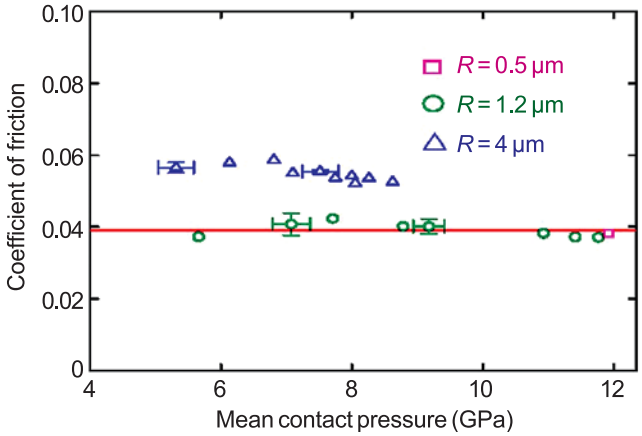

Figure 4: *Coefficient of friction between Si (100) surface and three diamond tips used in the experiments, as a function of mean contact pressure.*

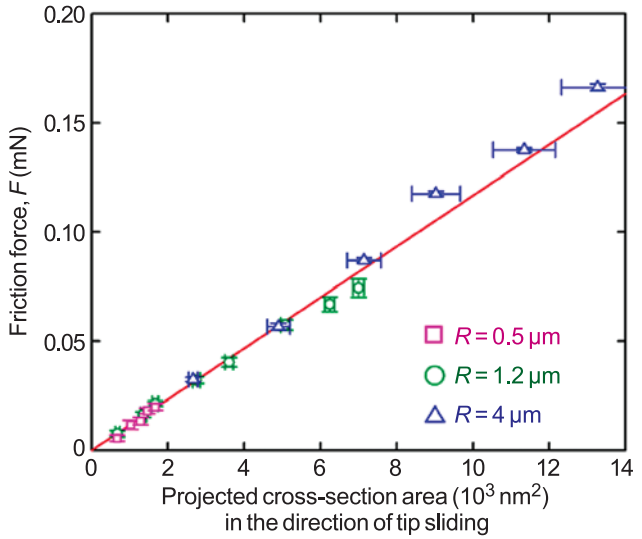

Figure 5: *Friction force as a function of projected cross-section area in the direction of tip sliding.*

This work shows clearly that nanoscale friction, in practice, is a complex result of both elastic and inelastic strains and deformations, and accurate nanofriction measurement will require careful accounting of all the forces contributing to the phenomenon. The methodology established in this work provides a substantial step towards the data and understanding needed by industry.

For More Information on this Topic

Z.C. Ying, S.M. Hsu (Ceramics Division, NIST)

Metrology for Nanoscale Properties: Brillouin Light Scattering

Brillouin light scattering is being employed to provide information on acoustic and magnetic waves at gigahertz frequencies in thin-film materials. Measurements and modeling in FY04 have focused primarily on interactions of spin waves in ferromagnetic films, elastic constants of nanoporous low-κ dielectrics, and propagation of acoustic waves in nanopatterned polymers.

Ward Johnson, Sudook Kim, and Colm Flannery

Technical Description

Brillouin light scattering (BLS) is an experimental technique that measures the intensity of spectral components of light that is inelastically scattered by vibrational waves (phonons) or spin waves (magnons) in a material. Fabry–Perot interferometric techniques are used to acquire accumulated spectra through repeated mechanical sweeping of the etalon spacing.

BLS is the only laboratory technique that is currently available for detecting magnons of finite wavenumber. Because of this capability and because of innovations in interferometric techniques, BLS has been increasingly applied to problems in magnetics over the past couple of decades.

For characterization of phonons in thin films, BLS offers several advantages over other techniques. Since it detects phonons in the gigahertz range, elastic constants can be determined in films of submicron thickness without the complication of vibrational energy penetrating significantly into the substrate. Modes localized in submicron structures can be characterized. Spatial variations in elastic properties and vibrational patterns can be measured with a lateral resolution equal to the size of the laser focal spot on the specimen (typically, ~50 micrometers).

In this division, techniques are being developed for characterizing interactions of magnons in metallic ferromagnetic thin films. Such interactions limit the speed of magnetic-storage devices, spin-valve sensors, and other thin-film magnetic devices.

BLS measurements and modeling of vibrational modes are being pursued in several thin-film systems, including nanoporous low-dielectric-constant (low-κ) dielectrics, nanopatterned polymers, and arrays of molecular rotors.

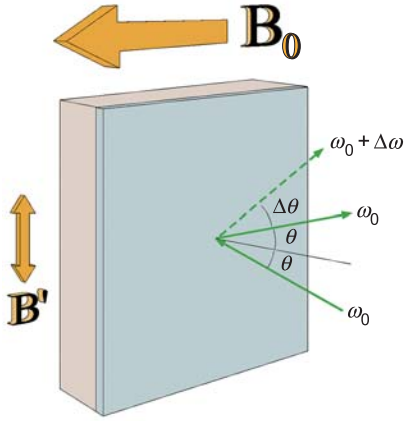

Figure 1: *Scattering of light off waves in a thin film.*

Accomplishments

During FY04, we developed and applied methods for measuring magnons that arise directly or indirectly from microwave pumping of metallic ferromagnetic films in a static magnetic field (Figure 1). BLS spectra were studied as a function of scattering angle, microwave power, and laser power to provide information on magnon–magnon interactions in $Ni_{81}Fe_{19}$. The results demonstrate, for the first time, detection of nonzero-wavevector magnons arising from the decay of pumped uniform-precession magnons in metallic thin films.

Young's modulus and Poisson's ratio in nanoporous low-κ dielectric films were measured using conventional backscattering techniques. This research is described elsewhere in this annual report.

Measurements and modeling of vibrational modes in nanoimprinted polymers were pursued in collaboration with the University of Akron and the NIST Polymers Division. In addition to bulk and surface modes, low-frequency modes were detected and found to be consistent with vibrational localization in the imprinted lines. This result suggests the possibility of characterizing elastic properties on a scale of tens of nanometers.

Contributors and Collaborators

P. Kabos (Radio-Frequency Technology Division, NIST); S. Russek (Magnetic Technology Division, NIST); A. Slavin (Oakland Univ.); J. Michl (Univ. of Colorado, Chemistry Dept.); R. Horansky (Univ. of Colorado, Physics Dept.); C. Soles (Polymers Division, NIST); R.H. Hartschuh, A. Kisliuk, and A. Sokolov (Univ. of Akron)

Physical Properties of Thin Films and Nanostructures: Green's-Function Methods

Precise knowledge of atomistic configuration and strains in nanomaterials is needed for their characterization and development of new devices. We have developed computationally efficient Green's-function methods for calculation of lattice distortion, elastic strains and displacements in a variety of material systems. Our work is useful for interpretation of data obtained by AFAM, nanoindentation, and SAW experiments.

Vinod K. Tewary and Bo Yang

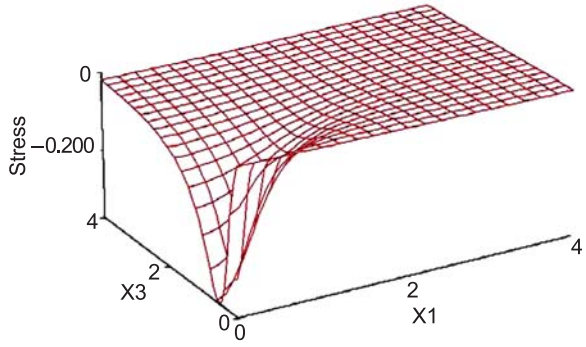

Figure 1: *Stress distribution in Si due to a surface load.*

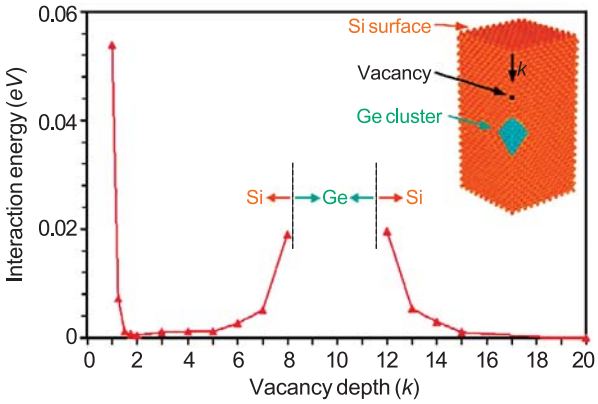

Figure 2: *Interaction energy of a cluster of 147 Ge atoms with a vacancy and free surface in Si.*

Technical Description

Green's function (GF) provides a computationally efficient tool for interpretation of data obtained by nanoindentation and atomic force acoustic microscopy (AFAM) which is useful for elastic characterization of nanomaterials. The dynamic GF is used for modeling propagation of surface acoustic waves (SAWs) in solids and their phonon properties. The GF accounts for interfaces and free surfaces in the solid and its elastic anisotropy, which play relatively important roles in the elastic response of nanomaterials as compared to ordinary solids. We use GF to calculate the elastic displacement fields, interaction energy between the embedded nanostructure and other defects and free surfaces. The displacement field, due to a force at the surface, is used for interpretation of AFAM and nanoindentation measurements. The interaction energy of the nanostructures is an important factor in the stability and growth of the nanostructure.

We have developed GF methods both at the discrete atomistic and macro continuum scales. For a lattice model containing N atoms, the GF is given by:

$$\mathbf{G} = \mathbf{\Phi}^{-1}$$

where $\mathbf{G}$ and $\mathbf{\Phi}$ are $3N \times 3N$ matrices of GF and force constants respectively. The matrix inversion is carried out by using the discrete Fourier transform for a perfect lattice or numerically by computer simulation for a model crystallite as in molecular dynamics.

In order to model an embedded nanostructure in a host solid, or a thin film on a substrate, we define an initial GF for the host and the final GF. The final GF is related to the initial GF through the Dyson equation.

In the continuum model, we simulate free surfaces and interfaces by applying the usual boundary conditions.

Accomplishments

We have carried out a detailed analysis of SAW measurements in a thin TiN film on Si, calculated stresses in a wide range of solids, and modeled Ge clusters in Si containing a free surface and a vacancy. The work is reported in six papers. A library of GFs is available at **www.ctcms.nist.gov/gf**, which contains downloadable teaching and tutorial material on GFs and computer codes for calculation of GFs. A GF group of about 50 international users has been formed at CTCMS.

Contributors and Collaborators

D. Hurley, D.T. Read (Materials Reliability Division, NIST); L. Bartlolo (Kent State University); A. Powell (M.I.T.)

Combinatorial Adhesion and Mechanical Properties: Axisymmetric Adhesion Testing

Axisymmetric adhesion tests promise a powerful means to quantify adhesive performance with the simultaneous ability to visualize debonding mechanisms. However, industrial adoption of these techniques has been slow, since traditional axisymmetric testing equipment does not allow rapid assessment of product performance over a large parameter space. In response, we are developing instruments that permit high-throughput (and high value) measurements of adhesion across combinatorial libraries.

Aaron M. Forster and Seung-ho Moon

Adhesion is governed by surface interactions and the mechanical properties of the adhesive. Axisymmetric adhesion (ASA) measurements, such as JKR[1] methods and "probe tack" tests, provide powerful means for quantifying these contributions to adhesion, while providing visual insight into the mechanisms by which adhesives fail. However, current ASA instruments are geared towards serial testing of single specimens. This "one-at-a-time" paradigm is incompatible with industry research, which increasingly requires methods to rapidly and thoroughly measure large numbers of adhesive formulations. Our objective is to produce ASA measurement instruments that operate in a high-throughput manner, while retaining the high-value data these methods produce. These tools enable the rapid identification of structure–property relationships critical for adhesive performance, thereby assisting industry in developing new adhesive formulations. This report describes two of the high-throughput ASA instruments that have been built to address these issues.

The JKR method employs a hemispherical lens that is pressed into a specimen. Tracking the lens/specimen contact area versus load or lens displacement yields the work of adhesion. Our instrument, the Multilens Combinatorial Adhesion Test (MCAT) employs an array of microlenses to conduct multiple JKR-type adhesion tests in parallel. By simultaneously tracking the contact radii of each element of the lens array, up to 400 measurements of the work of adhesion are collected in the time required for a single traditional JKR test (see Figure 1). When MCAT is used in conjunction with gradient combinatorial specimen libraries, each lens measures a different adhesive system. We recently benchmarked MCAT measurements of the work of adhesion between glass and silicone against single lens JKR tests, with excellent agreement.

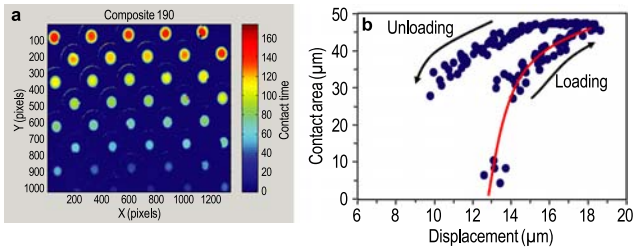

Figure 1: *a) Contact area map of MCAT lens array. Each circle represents data for a separate measurement. b) Contact area vs. displacement data for a single lens array element. The red line is the fit to JKR theory, which yields the work of adhesion.*

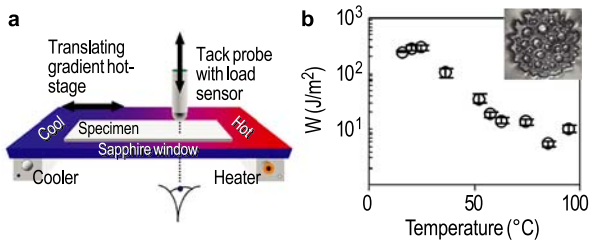

Figure 2: *a) Schematic of CPT adhesion test instrument. b) Adhesion energy (W) of a model PSA vs. temperature. Inset: Image of probe/sample contact shows debonding of the PSA.*

The adhesion of viscoelastic materials, such as pressure sensitive adhesives (PSAs), is not described well by JKR-type tests. Probe tack tests provide quantitative adhesion measurements for viscoelastic systems with simultaneous visualization of debonding events. We developed a new combinatorial probe tack (CPT) test for the measurement of PSA formulation performance (Figure 2). A key feature of the instrument, a gradient hot-stage, enables rapid assessment of temperature effects. Temperature is an important processing parameter and environmental factor for PSAs. Our CPT testing of PSAs (Figure 2) rapidly provides quantitative adhesion energy data and debonding images as a function of temperature. The device design significantly reduces experimental uncertainties associated with fabrication of multiple samples, and reduces the overall measurement time significantly, while maintaining high-quality, rich datasets. We are currently refining the CPT instrument and testing its use towards a variety of applications such as UV-cured PSAs and epoxy systems.

Reference

1. K.L. Johnson, K. Kendall, and A.D. Roberts, *Proceedings of the Royal Society of London A: Materials* **324**, 301 (1971).

Contributors and Collaborators

A. Chiche, C.M. Stafford, W.L. Wu, W. Zhang (Polymers Division, NIST)

Combinatorial Adhesion and Mechanical Properties: Innovative Approaches to Peel Tests

Peel testing is the primary tool industry uses to gauge adhesive performance, but current peel test methods involve "one-at-a-time" analysis of single specimens. Our research aims to accelerate adhesive performance testing by developing devices and measurement strategies that meld the peel test construct with combinatorial and high-throughput (C&HT) methods.

Christopher M. Stafford and Martin Y.M. Chiang

As part of the mission of the NIST Combinatorial Methods Center (NCMC), we are developing C&HT peel-test methods that enable rapid assessment of adhesion within the large parameter space associated with adhesive formulation and processing. This report describes two milestones we have met in this endeavor.

Our first achievement involves a NIST-developed experiment design for measuring adhesion of a polymer layer to an underlying substrate in a combinatorial manner. This test method utilizes the peel-test geometry to investigate the interfacial failure between a thin polymer film and a silicon substrate as a function of annealing time and temperature, as well as the substrate surface energy. Combinatorial libraries are generated by using the existing NCMC gradient toolkits: a polymer film is coated onto a substrate containing a surface energy gradient, and this sample is subsequently exposed to an orthogonal temperature gradient.[1] To further extend the parameter space available in this study, we incorporated annealing time as a third dimension. This requires fabricating multiple identical samples and successively annealing each sample for longer times. By applying the Williams–Landel–Ferry (WLF) time-temperature superposition, we can construct a master curve (failure map) detailing the transition from adhesion (bonded) to failure (debonded) as a function of substrate surface energy, annealing time, and annealing temperature (see Figure 1). This defines an operating window of temperature, time, and surface energy to ensure proper adhesion of a thin polymer film to the material of interest.

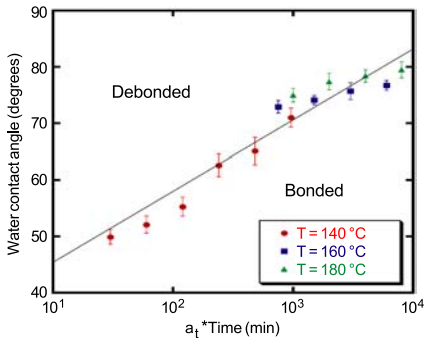

Figure 1: *Master adhesion map delineating critical surface energy conditions for adhesion vs. a reduced time-temperature function, a_t.*

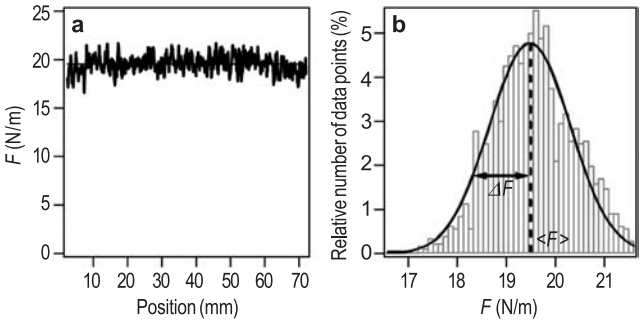

Figure 2: *a) Force vs. distance curve for a typical peel test; and b) distribution curve of the force data.*

Our second achievement addresses a challenge in applying the peel test to combinatorial specimens: the lack of ample statistical information that is the foundation of this type of measurement. For example, a conventional peel test conducted under constant conditions results in a fluctuating force to be averaged. Applying a continuous gradient of sample properties or test conditions in the peel direction implies that each data point (force) corresponds to a given test condition, thus prohibiting the average force to be calculated for a given condition. To address this issue, we have developed a simple statistical treatment that allows a relationship between the uncertainty of the force and the domain size to be established. This treatment ultimately will dictate the number of data points required to obtain acceptable uncertainties in the measurement.

These studies demonstrate how combinatorial approaches can be applied to characterize adhesion using a peel test blueprint. In doing so, we have designed a new statistical tool to assist in defining the gradient step size (discrete gradients) or gradient steepness (continuous gradients) that allows ample statistical information to be obtained.

Reference

1. For details, see A. Seghal, *et al., Microscopy Today* **11** (6), 26–29 (2003).

Contributors and Collaborators

A. Chiche, R. Song, A. Karim (Polymers Division, NIST); J. Filliben (Statistical Engineering Division, NIST)

Thermochemistry and Metrology of Interfacial Interactions

Reactions occurring at interfaces during the high-temperature processing of complex electronic materials involve diverse chemical compositions. To optimize the design and control of these interfaces, we are developing a generic thermodynamic/kinetic model for interfacial interactions. The model includes modification of bulk reaction and mass transport parameters to accommodate nanoscale observations.

Lawrence P. Cook, Winnie Wong-Ng, and Igor Levin

State-of-the-art electronic devices contain complex materials with chemical constituents ranging widely over the periodic table; furthermore, new materials are continually being added. Many electronic packaging materials consist of metals, ceramics, and semiconductors, with bi-phasic interfaces of several types. Processing temperatures may extend up to 900 ºC where diffusion and reaction can be significant. Two principal problems arise in the treatment of such interactions: 1) the application of equilibrium thermodynamic data to the non-equilibrium growth of interfacial reaction zones, and 2) the transition from micro-scale (bulk dominated), to nanoscale (surface dominated) phenomena. To address these issues, we have instituted a combined thermodynamic/kinetic approach to investigate the model system Ag-Bi_2O_3-Nb_2O_5-O, as outlined in Figure 1.

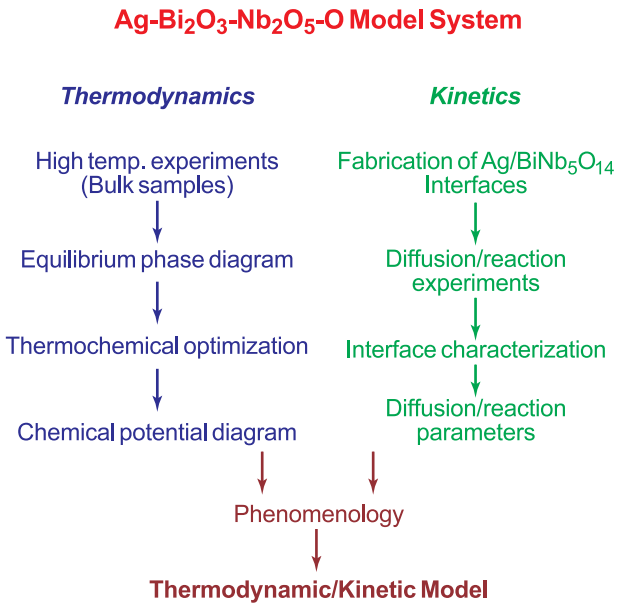

Figure 1: *Flow chart for development of interfacial model based on Ag-Bi_2O_3-Nb_2O_5-O.*

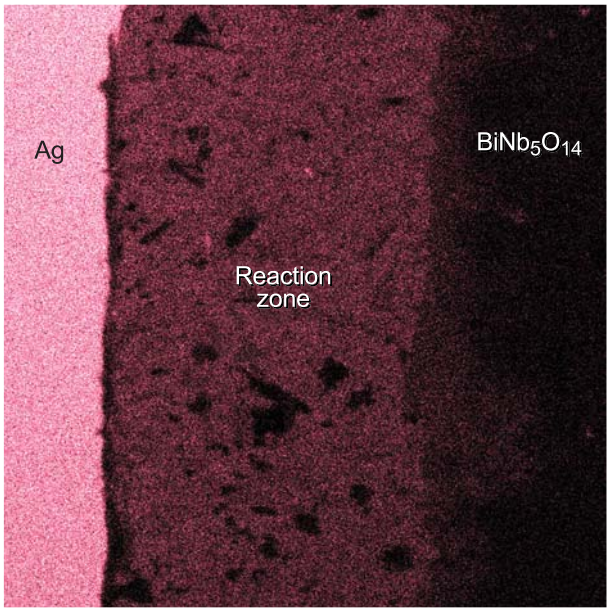

Figure 2: *Ag L_α X-ray map of Ag/$BiNb_5O_{14}$ reaction zone (≈ 80 μm wide) produced by annealing in air for 10 h at 850 ºC, with an applied uniaxial compression of ≈ 1 MPa.*

Progress includes determination of a preliminary phase diagram at 850 ºC, and development of a provisional thermodynamic model. Subsequent construction of a chemical potential diagram has allowed us to predict alternative diffusion and reaction paths. Observations on Ag/$BiNb_5O_{14}$ reaction couples (Figure 2) confirm the relatively high thermodynamic mobility of Ag. Thermogravimetric data on the interfacial reaction require more than a simple parabolic rate law, due to the rapid initial spread of Ag along reaction site surfaces. By comparison with particulate interfacial systems, a two-step reaction model is proposed, for which rate constants can be obtained.

Data for the model system are of direct interest to the electronics community because Ag is an important metallization component in many dielectric ceramics. It is anticipated that continued work on Ag-Bi_2O_3-Nb_2O_5-O will lead to the goal of a comprehensive thermodynamic/kinetic model. The model will be tested, iteratively refined, and extended to other systems.

Contributors and Collaborators

M.D. Vaudin, P.K. Schenck, T. Vanderah, M. Green (Ceramics Division, NIST); W. Luecke (Metallurgy Division, NIST); C. Randall, M. Lanagan (Center for Dielectric Studies, Pennsylvania State University)

Chemistry and Structure of Nanomaterials

Successful nanoscale materials fabrication is empowered by a detailed knowledge of the chemistry and structure of surface bound molecules; e.g., the optimization of self-assembled monolayers, molecular templates, micro-electro-mechanical system lubricants, and functionalized nanotubes. Near-Edge X-ray Absorption Fine Structure (NEXAFS) spectroscopy is ideally suited to measure non-destructively chemical bond concentration, rehybrization, and orientation with sub-monolayer molecular sensitivity in diverse nanoscale materials. Furthermore, NEXAFS can distinguish chemical bonding in the light elements, measure the orientation of interfacial molecules, and separately measure surface versus bulk chemistry simultaneously.

Daniel A. Fischer

Materials having low energy surfaces are used in many applications, for example, in non-wetting surfaces or fouling resistant marine coatings. We have produced a photo-responsive polymer surface by combining the reversible photo-switching nature of azobenzene with the self-assembly nature and low surface energy properties of semi-fluorinated segments, to create a fluoroazobenzene molecule surface. Upon UV exposure, this surface reorients between hydrophobic and less hydrophobic states, as shown in Figure 1 (left upper and lower panels). For such surfaces, one could imagine applications ranging from low cost surface patterning to polymer surfaces that would adsorb biological macromolecules on cue.

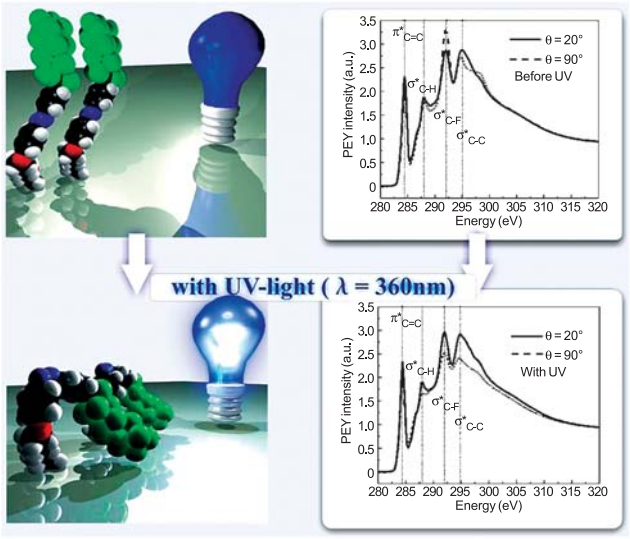

Figure 1: *UV light reorients fluorobenzene semi-fluorinated segments (green) downwards, i.e., to a less hydrophobic state.*

We have utilized NEXAFS to observe, verify, and quantify the reversible cis-trans molecular conformation transformation from hydrophobic to less hydrophobic states. The right panels of Figure 1 (upper and lower) show polarization dependent NEXAFS anisotropy behavior of the C–F and C–C peaks which reverse with *in situ* UV light exposure highlighting the reorientation of the semi-fluorinated segments.

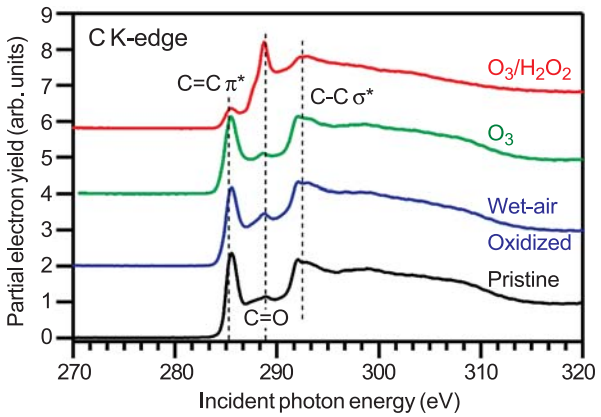

Figure 2: *Carbon NEXAFS of oxidized/functionalized nanotubes.*

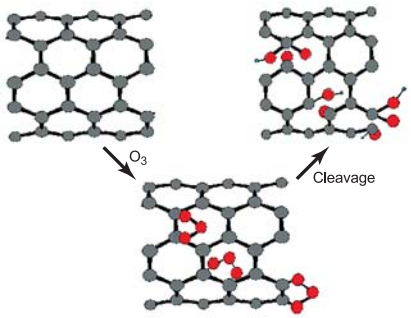

Figure 3: *Model of peroxide functionalization of nanotubes.*

Application of NEXAFS spectroscopy to the study of electronic structure and chemical composition is illustrated in Figure 2 for various chemically functionalized, single-walled, carbon nanotubes. Upon peroxide functionalization, the C=C ring resonance is greatly diminished on extensive sidewall functionalization indicating loss of extended conjugation and disruption of nanotube electronic structure. The C=O peak intensity is greatest for peroxide chemistry. NEXAFS spectroscopy supports a model of peroxide funtionalization, shown in Figure 3.

Contributors and Collaborators

S. Samabasivan (Ceramics Division, NIST); X. Li, C.K. Ober (Cornell); A. Hexemer, E.J. Kramer (UCSB); S. Banerjee, T. Benny, S.S. Wong (SUSB); J.A. Misewich (BNL)

Metrology for Nanoscale Properties: X-ray Methods

Macroscopic properties of technologically interesting materials originate from their underlying micro-structure. To design and understand improved materials, it is necessary to characterize the microstructure and correlate its changes to the macroscopic properties of interest. We especially focus on x-ray diffraction studies of biomedical, ferroelectric, optoelectronic, photovoltaic, semi-conducting, and other materials relevant to the health and microelectronics industries. In particular, studies of microstructural properties, such as strain and stress, crystalline defects, and texture, complement the information obtained by other techniques.

Thomas A. Siewert and Davor Balzar

In this report, we focus on two topics: the studies of superconducting tungsten thin films and comparison of the thin-film texture, as obtained by Electron Back Scatter Diffraction (EBSD) and x-ray diffraction (XRD). Tungsten superconducting transition-edge sensors (TES) are used in different astrophysics and astronomy applications, and as single-photon detectors for the quantum computing experiments. Such detectors comprise thin tungsten films and operate at temperatures close to absolute zero and to the critical superconducting transition temperature (*Tc*) of tungsten. Thin films, in general, contain both high-temperature α-W phase (with *Tc* = 15 mK) and β-W (A15 cubic structure with *Tc* = 1–4 K). Close to the *Tc*, very small thermal changes, such as the absorption of a single photon, increase the film electrical resistance. The result is the production of an electrical output signal that corresponds directly to the detection of the absorbed photon energy. In general, residual stress can influence the *Tc* of the thin film both directly and by inducing the β→α phase transformation. Thus, in order to control the *Tc*, it is necessary to measure and control both the phase composition and residual stresses. Residual stresses in films depend on the preparation conditions, the thickness of the film, and the difference in thermal expansion coefficient between the film and the substrate. The total residual stress results from both the intrinsic (growth) stress and thermal stress. We measured the stress by XRD at both ambient and cryogenic temperatures. The sample was held in a continuous flow cryostat that was capable of achieving temperatures as low as 8 K. The cryostat was mounted on a goniometer to enable the angle-dispersive XRD measurements. The shift of the α-W {110} Bragg reflection was used to estimate stress at 8 K, and directional measurement of the {321} lattice spacings ($\sin^2\psi$ method) yielded the total residual stress at ambient temperature. The values obtained are about 0.7 GPa and higher, where the bulk of the stress is due to the intrinsic (growth) component.

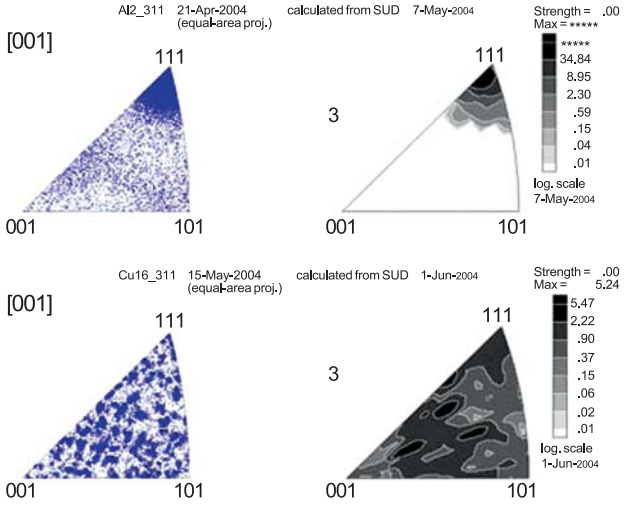

Figure 1: *EBSD (left) and XRD (right) inverse pole figures of aluminum (top) and copper (bottom) thin films.*

Texture has a large influence on many properties of thin films. XRD was the primary method for the characterization of texture for many years. Recently, alternative local techniques have been developed to bring the measurements to the nanoscale. This year, we compared measurements taken with conventional XRD and EBSD on two thin films: sputtered aluminum and electroplated copper. Both films had a thickness of about 1 μm and were grown on [100] silicon wafers. The inverse pole figures for both samples and techniques are shown in Figure 1. It is obvious that the agreement between XRD and EBSD in case of aluminum film is very good, whereas it is rather poor for copper film. This is a consequence of different penetration depths of electrons and x-rays; while the aluminum sample is homogeneous through the film thickness, copper film is not. After sample preparation, electroplated copper is likely to undergo self-annealing at room temperature. This well-known phenomenon yields a difference in grain size and orientation between the surface and the bulk of the sample.

Contributors and Collaborators

Adriana Lita, Jens Müller, Roy H. Geiss, Dave T. Read, M. Kopycinska–Müller, Robert Keller (NIST); Laurna Kaatz, Amitendra Chaudhuri (University of Denver)

Physical Properties of Thin Films and Nanostructures: Grain Size Effects on Actuator Fatigue

Several materials are now produced commercially with particle sizes on the order of 10–100 nm. The availability of ceramic materials in this size classification is particularly important for the electronic component industry. Nanopowders can enable significant decreases in internal layer thickness (for multilayer devices), minimize the size and prevalence of processing defects, and boost the overall performance of components ranging from capacitors to resistive gas sensors. Quantifying these performance enhancements and their dependence on microstructure is a key objective in the Materials Reliability Division.

Stephanie A. Hooker

Many multilayer ceramic devices can benefit from the use of ultra-fine powders, including passive electronic components, gas sensors, and miniature actuators. However, fabrication issues associated with processing these high-surface-area powders have hindered their commercialization. Key challenges have included nanopowder reproducibility, optimization of processing slurries, and control of sintering profiles to produce the desired micro/nanostructure characteristics. Moreover, in many cases, predicting the optimum microstructure features for maximum performance is quite difficult, and extensive experimentation remains necessary.

One specific component that can benefit from the use of nanopowders is the multilayer piezoelectric actuator. These devices generate precise, controlled motion for translating optics, damping vibrations, redirecting air flow, and dispensing fluids. Each component consists of many active layers, the thickness of which determines the device's power requirements. Layer thickness is typically on the order of several hundred microns for conventional actuators and is driven by the need for many individual piezoelectric grains to span the active layer, thereby reducing the chance for electrical failure. Reducing grain sizes from micrometer to submicrometer scales enables dramatic decreases in layer thickness, reducing power needs and increasing applicability.

However, at issue is the piezoelectric response and, in particular, the long-term fatigue resistance. Fatigue is the change in polarization or displacement over time and is a recognized problem for state-of-the-art actuators. Because processing-induced defects tend to be on the scale of the starting powder, nanopowders can improve mechanical durability. However, a corresponding decrease in ferroelectric response is also anticipated as grain size reduces. Fatigue is affected by both the mechanical and electrical responses, making its prediction quite difficult for fine-grained components.

In FY04, we investigated the fatigue behavior of 14 microstructures obtained by controlled sintering of 80-nm PZT-5A powders. The devices tested were 1206-sized (0.30 cm × 0.15 cm, or 0.12″ × 0.06″) chips, each with 10 active layers (50 μm thick). Characterization included dielectric, impedance, and ferroelectric properties, as well as short- (<1 million cycles) and long-term (1–100 million cycles) degradation under combined electrical and mechanical influences.

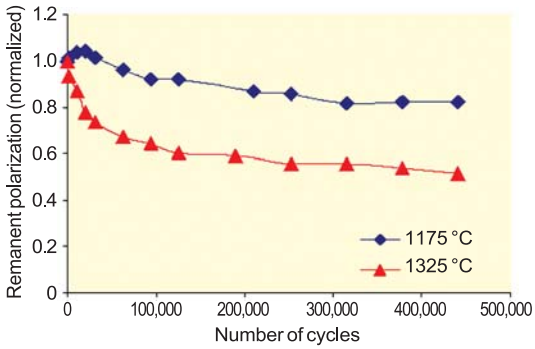

Figure 1: *Effect of sintering temperature on ferroelectric fatigue.*

The results clearly demonstrate the dependence of fatigue on microstructure. Figure 1 compares changes in remanent (*i.e.*, permanent) polarization over time when devices were cycled using a 35 Hz sinusoidal wave with an amplitude of +/–75 V. The average decrease in polarization for the finest-grained materials (sintered at 1175 °C) was less than 20 % after 0.5 million cycles, compared to nearly 50 % for larger-grained components.

In FY05, we will expand on this work and examine the corresponding effects on displacement and domain reorientation for devices with even thinner internal layers. The resulting data will then be used to validate the suitability of these components for biomedical and smart structures applications, both of which demand high performance and long operational lifetimes.

Contributors and Collaborators

R. Geiss (Materials Reliability Division, NIST); C. Kostelecky, D. Deininger, K. Womer (Synkera Technologies)

Physical Properties of Thin Films and Nanostructures: Nanoporous Low-κ Dielectric Films

Nanoporous low-dielectric-constant (low-κ) films present considerable implementation challenges for the microelectronics industry and also raise new scientific questions. We apply optical methods to these films to evaluate such critical properties as density/porosity, Young's modulus, and Poisson's ratio. Our techniques allow measurement of properties that are otherwise difficult to determine and shed light on how the mechanical properties depend on porosity.

Colm Flannery and Donna C. Hurley

Current miniaturization trends in microelectronics require faster device switching. This need can be at least partially met by lowering the resistance-capacitance factor of the dielectric materials. One promising solution is to introduce nanometer-sized pores that reduce the dielectric constant κ. Unfortunately, introduction of porosity may lead to a drastic reduction in stiffness (Young's modulus), adversely affecting the material's chances of surviving the fabrication process. In addition to predicting and ensuring process reliability, accurate values of a film's mechanical properties are needed to model the mechanical behavior of the resulting microelectronics device. New tools are needed to characterize these relevant thin-film properties (*e.g.*, Young's modulus and Poisson's ratio ν), as well as to better define their dependence on porosity.

In FY04, we evaluated Poisson's ratio ν in methylsilsesquioxane (MSSQ) polymer films of varying porosity with Brillouin light scattering. In this technique, a Fabry–Perot interferometer detects frequency-shifted photons scattered by ambient thermal phonons in the material. The frequency shift of the photons is characteristic of the acoustic phonon modes in the film. Values of ν were determined from measurements of both longitudinal and surface acoustic wave modes. Figure 1 reveals that ν decreases as porosity increases. The results

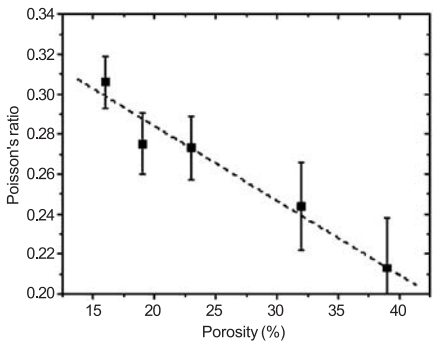

Figure 1: *Measured Poisson's ratio vs. porosity for MSSQ films.*

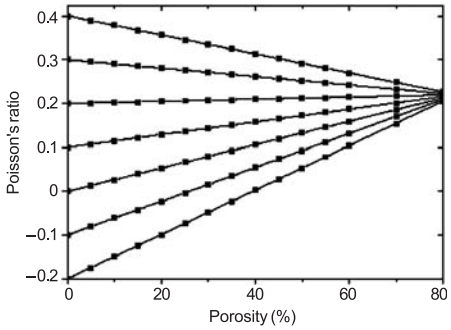

Figure 2: *Predicted dependence of Poisson's ratio on porosity.*

of an existing finite-element model, shown in Figure 2, predict that ν will either decrease or increase depending on the initial ν of the matrix material. In addition, ν tends towards a constant value of 0.2 for all materials at high porosity. Our measurements are consistent with the model. However, they show a much larger rate of decrease in ν, probably because a percolation threshold had been reached. Quantitative results like these will prove valuable for modeling of structures involving low-κ films. The results also yield insight into the porosity dependence of ν, about which very little is known.

A second method to determine thin-film properties involves the frequency-dependent dispersion of laser-generated surface acoustic waves (SAWs). In FY04, efforts concentrated mainly on the development of a standard SAW data analysis procedure. With careful signal processing that minimizes sensitivity to noise and maximizes the frequency range of the measured signals, we can extend the frequency range of our measurements by 20 %. The result is a significant reduction in the uncertainty of the extracted film properties. The method lends itself to automatation and has allowed us to inspect films less than 300 nm thick. (Previously, films less than 500 nm thick were challenging.)

The improved measurement procedure, combined with new multilayer Green's function analysis software, has allowed us to inspect multilayer structures. With these capabilities, we have extracted properties of thin (50–100 nm) capping layers of stiffer materials on top of more compliant functional films. In addition, the Young's modulus, density, and thickness of the underlying dielectric films were evaluated.

Contributors and Collaborators

S. Kim, V. Tewary (Materials Reliability Division, NIST); Y. Liu (International Sematech); J. Wetzel (Tokyo Electron America)

Nanoscale Characterization by Electron Microscopy

Electron microscopy is used to characterize the structure and composition of materials at the nanometer scale to better understand and improve their properties. New measurement techniques in electron microscopy are being developed and applied to materials science research. The MSEL Electron Microscopy Facility primarily serves the Metallurgy, Ceramics, and Polymers Divisions as well as other NIST staff and outside collaborative research efforts.

John E. Bonevich

Atomic-scale structure and compositional characterization of materials can lend crucial insights to the control of their properties. For instance, direct observation of local structures by transmission electron microscopy (TEM) provides important feedback to the optimization of crystal growth and processing techniques. Various characteristics may be observed such as crystal structure and orientation, grain size and morphology, defects such as stacking faults, twins, grain boundaries and second phase particles. Structure, composition and internal defect structures, as well as the atomic structure of surfaces and interfaces, can provide powerful knowledge for engineering and understanding materials.

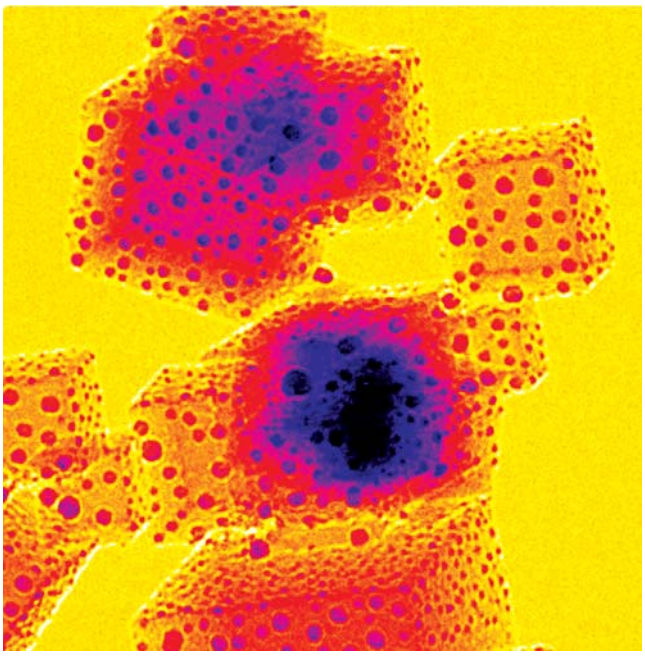

Figure 1: *MgO cubes with surfaces decorated by small gold particles. These particle ensembles are used in model studies of 3D chemical imaging at the nanoscale (electron tomography).*

The MSEL Electron Microscopy Facility consists of two transmission electron microscopes, three scanning electron microscopes, a specimen preparation laboratory, and an image analysis/computational laboratory. The JEM3010 TEM can resolve atomic structures and employs an energy selecting imaging filter (IF) and X-ray detector (EDS) for analytical characterization of thin foil specimens. The S-4700-II FE-SEM employs electron backscattered diffraction/phase identification (EBSD) and EDS systems to characterize the crystallographic texture and composition of materials.

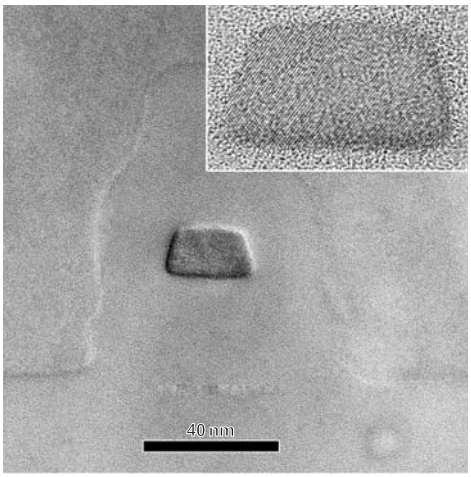

Figure 2: *Confined Si single electron transistor device.*

Highlights from the EM Facility for FY2004 include:

- A new, high-sensitivity EBSD CCD camera which acquires in excess of 70 patterns/second, was installed on the FE-SEM.
- 3D Chemical Imaging at the Nanoscale, a collaborative project with CSTL and PL on tomographic characterization of materials, was initiated (Figure 1).
- Research collaboration with the Semiconductor Electronics and Electricity Divisions (EEEL) has characterized quantum effects in confined Si devices (Figure 2).
- Sub-100 nm Ag interconnects formed by superconformal electrochemical deposition was characterized.

Contributors and Collaborators

D. Josell, T. Moffat, L. Bendersky (Metallurgy Division, NIST); I. Levin, B. Hockey (Ceramics Division, NIST); J.H.J. Scott (Surfaces & Microanalysis Science Division, NIST); Z. Levine (Optoelectronics Division, NIST); E. Vogel (Semiconductor Electronics Division, NIST)

Gradient Reference Specimens for Advanced Scanned Probe Microscopy

Engineering of nanomaterials, biomaterials, and nano-electromechanical systems hinges on techniques for imaging complex nano-structures. In this respect, new Scanned Probe Microscopy (SPM) methods promise nano-scale mapping of chemical, mechanical, and electro-optical properties, but these techniques generally only offer qualitative information. Through a suite of reference specimens fabricated with a combinatorial design, we aim to calibrate image data from emerging SPM methods, thereby advancing these nanometrology tools.

Michael J. Fasolka and Duangrut Julthongpiput

Recent years have seen the development of a new generation of SPM techniques, which intend to measure chemical, mechanical, and electro–optical properties on the nanoscale. However, contrast in new SPM images is difficult to quantify since probe fabrication can be inconsistent and probe/sample interactions are not understood. Our research at the NIST Combinatorial Methods Center (NCMC) aims to provide a suite of reference specimens for the quantification of next generation SPM data. By design, our specimens will gauge the quality of custom-made SPM probes, calibrate SPM image contrast through "traditional" surface measurements (*e.g.*, spectroscopy, contact angle) and provide information for understanding complex probe/sample interactions. Our specimens are produced with bench-top microfabrication routes and combinatorial gradient methods developed by the NCMC. Here, combinatorial methods are key since they enable the fabrication of specimens that vary properties that govern SPM image contrast in a systematic, independent manner. Moreover, as opposed to traditional reference specimens, combinatorial samples provide not one, but a multitude of calibration conditions.

Figure 1 illustrates principles of our specimen design through a specific case useful for quantifying chemically sensitive SPM techniques such as friction-force SPM,

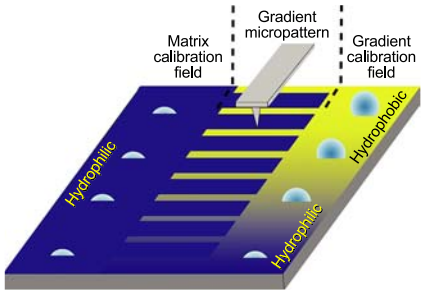

Figure 1: *Schematic illustration of our gradient reference specimen for chemically sensitive SPM techniques.*

or Chemical Force Microscopy, which employs a custom-made probe. The crux of this specimen is a "gradient micropattern" (∇-μp): a series of micron-scale lines that continuously change in their chemical properties (*e.g.*, surface energy) compared to a constant matrix. Two "calibration fields" adjacent to the ∇-μp directly reflect the chemistry of the lines and the matrix. Thus, traditional measurements (*e.g.*, contact angle) along the calibration fields (1) gauge local chemical differences in the ∇-μp and thereby (2) calibrate contrast in SPM images acquired along the ∇-μp.

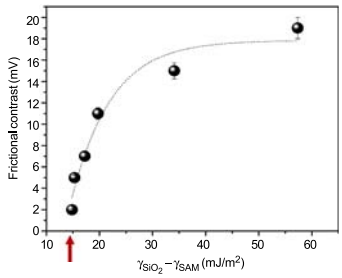

Figure 2: *Preliminary calibration curve relating friction force SPM image contrast to differences in surface energy (γ), as determined from a single gradient reference specimen. The minimum contrast point (red arrow) illuminates the sensitivity of the probe.*

Figure 2 demonstrates use of this specimen for calibrating friction force SPM image contrast. We fabricate this specimen via microcontact printing of a chlorosilane self-assembled monolayer (SAM) on a SiO_2 matrix. The chemical gradient is achieved via a graded UV-ozonolysis of the SAM. The plot abscissa gives the difference in friction force (contrast) between the lines and matrix for SPM images collected along the ∇-μp. The ordinate expresses the corresponding surface energy (γ) data (from contact angle measurements) collected along the calibration fields. Thus, from a single specimen we create a comprehensive calibration curve that relates SPM friction force to differences in surface energy. Moreover, the plot neatly illuminates the smallest γ difference sensed by the probe (red arrow), which is useful for gauging the quality of custom-made probes.

Currently, we are refining this reference specimen design, and we are developing similar designs for other advanced SPM methods.

Contributors and Collaborators

K. Beers (Polymers Division, NIST); D. Hurley (Materials Reliability Division, NIST); T. Nguyen (Materials and Construction Research Division, BFRL); S. Magonov (Veeco/Digital Instruments)

Characterization of Counterion Association with Polyelectrolytes: Novel Flexible Template Behavior

Polyelectrolytes differ in chain dynamics and equilibrium structure from neutral polymers due to long-range electrostatic interactions. This manifests into strongly interacting solutions for both synthetic and biopolymers, as observed by associative behavior and multi-mode relaxations. Origins of these relaxations require new experimental methods probing the local structure and dynamics.

Vivek M. Prabhu and Eric J. Amis

Polymeric templates are found throughout nature most commonly in the nucleic acid base-pairing of DNA. This special hydrogen bond template has currently been explored for design of novel nanostructured materials. New routes to self-assembled or template-assisted assembly using externally supplied fields such as electric, flow, magnetic, and patterned substrates must overcome Brownian motion as well as structural correlations between and among molecules. For polyelectrolytes, such as DNA, the long-ranged electrostatic interactions also contribute to the solution structure in addition to the local and directional hydrogen bond associations. The distribution and dynamics of the counterion species about a polyelectrolyte serve as a starting point to understand the interactions governing controlled assembly and complement the often-studied polymer structure point-of-view.

We have established, using neutron scattering experiments performed at the NIST Center for Neutron Research (NCNR), the remarkable ability for counterions to essentially conform to linear flexible polyelectrolytes. This was accomplished by direct measure of the counterion partial static and dynamic structure factor highlighting the coupled polymer and counterion association for model synthetic materials shown below.

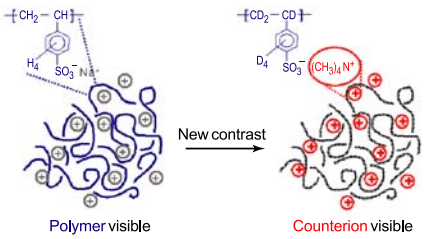

Small-angle neutron scattering (SANS) was used to characterize the equilibrium structure, while neutron spin echo (NSE) spectroscopy was used to examine the dynamics occurring at length scales between (60 and 3) nm and time scales between 45 ps to 100 ns.

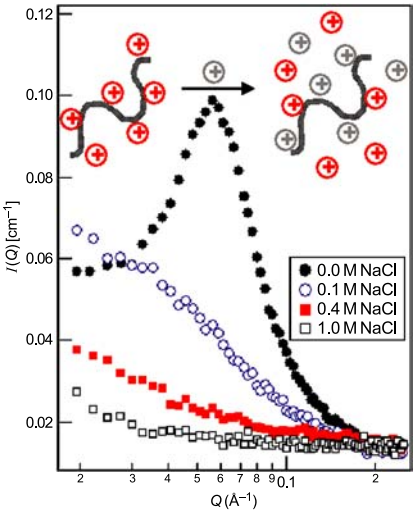

Figure 1: *"Visible" organic counterions associate with the negatively charged chain at low salt and are displaced by added "invisible" sodium ions for fixed polymer concentration of 24.9 gL^{-1}.*

An example of the counterion correlations is shown by the SANS structural peak in Figure 1. The peak illustrates the counterion correlations mediated by the chain. By tuning the range of the electrostatic interactions with added NaCl, an "invisible" salt, the influence is two-fold: (1) the electrostatics are screened, and the solution returns to neutral-like behavior; and (2) at higher salt concentrations, the Na^+ displace the visible *h*-TMA^+ counterions as shown in the accompanying schematic. Although the polymer template is no longer observed, its influence is still observed with a "visible" salt.

The counterion dynamics are length scale dependent and slow down near the correlation peak. This behavior illustrates that the polyion-counterion motions are coupled at the nanoscale. Hence, the role of counterions also serves as a design criteria in assembling structures. Unique labeling has provided a new viewpoint of charged polymer solution structure and dynamics. This project aims to characterize the role of charged polymer topology with branched materials, networks, and gels on the coupled dynamics to assess the parameters governing template-assisted assembly. Modern simulation and theoretical insight will assist in understanding these challenges for nanoscale assembly.

Contributors and Collaborators

D. Bossev, N. Rosov (NIST Center for Neutron Research)

Grand Challenges in Nanomagnetics: High Coercivity FePt Alloys for Future Perpendicular Magnetic Data Storage

The magnetic data storage industry is seeking to sustain the 30-year trend of exponentially increasing storage density. This must be achieved at the same time as maintaining the stability of the recorded data. The Metallurgy Division at NIST is collaborating with Seagate Technology to develop the processes required to produce patterned media of high-magnetic coercivity that will meet this challenge.

Jonathan J. Mallett, Thomas P. Moffat, and William F. Egelhoff, Jr.

Conventional magnetic data storage media are based on granular films in which many fine grains are used to define each magnetic bit. The minimum number of grains per bit is limited by the irregularity of the shape and spacing of the grains, which produces irregular boundaries between bits. This irregularity results in noise in the read signal and can only be constrained at an acceptable level by maintaining a fixed minimum number of grains per bit. The natural approach to increasing data storage density has been to reduce the grain size, while maintaining the same number of grains per bit. The limit to this approach occurs when the magnetic energy barrier to the reversal of magnetization of each grain approaches the energy of random thermal fluctuations. At this point, the medium is no longer stable against spontaneous magnetization reversal and consequential data loss.

The grain size at which this limit occurs depends on the magnetocrystalline anisotropy energy of the magnetic material. FePt in its $L1_0$ phase has a sufficiently large anisotropy energy to allow magnetically stable grains of 5 nm diameter (Figure 1). Furthermore, FePt deposited by a variety of means typically forms grains approaching this size. Unfortunately, the annealing treatment required to transform the as-deposited A1-structured FePt to the desirable $L1_0$ phase is widely found to result in an increase in grain size to 100 nm. Current efforts at NIST focus on developing a method of electrochemically depositing FePt into a regular patterned template, circumventing the problem of grain growth. Simultaneously, the imposed regularity of the magnetic cells opens the possibility of addressing single cells (*i.e.*, of using one "grain" per bit). The estimated achievable density from such an approach is 7 Tbits per square inch, which is 100 times higher than current storage densities. Electrodeposition is an obvious choice for deposition into high aspect ratio templates, since it does not suffer from the shadowing effect that characterizes vacuum deposition techniques.

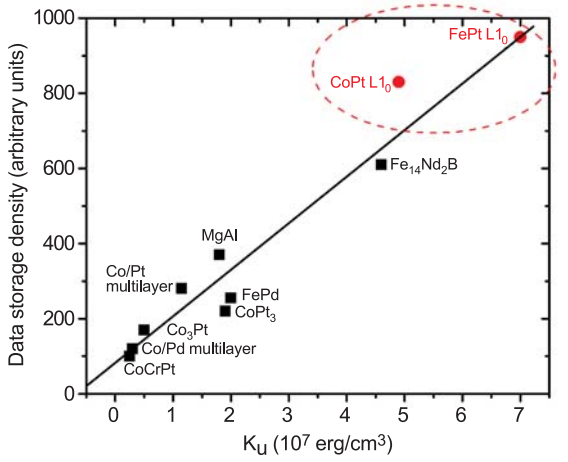

Figure 1: *The dependence of storage density on magnetocrystalline anisotropy energy. The most promising materials are FePt and CoPt.*

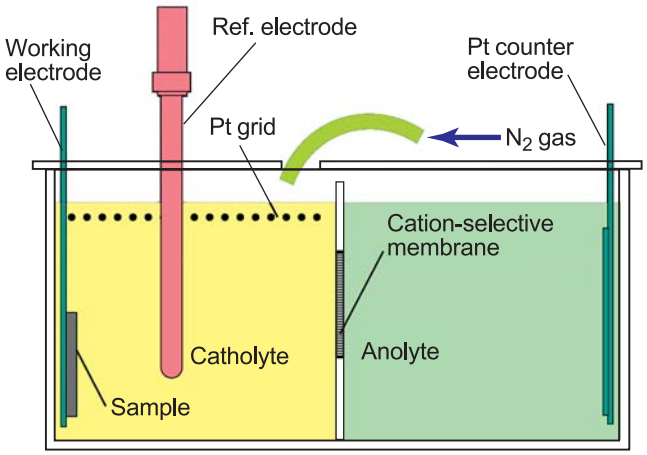

Figure 2: *The double cell, designed to minimize the concentration of Fe^{3+} and dissolved O_2 in the FePt plating solution.*

Electrodeposition of FePt from aqueous solutions presents many challenges. The double cell shown in Figure 2 has been developed to address the problem of the instability of Fe^{2+} solutions, which readily oxidize to produce insoluble $Fe(OH)_3$. The plating solution, containing $FeCl_2$ and $PtCl_4$ (left) is separated from the anode by a cation selective membrane, preventing the oxidation of Fe^{2+} to Fe^{3+} that would otherwise occur at the anode. Fe^{3+} formation by oxidation with air is also minimized by blanketing the cell in nitrogen, and residual Fe^{3+} is reduced to Fe^{2+} by an auxiliary platinum grid electrode.

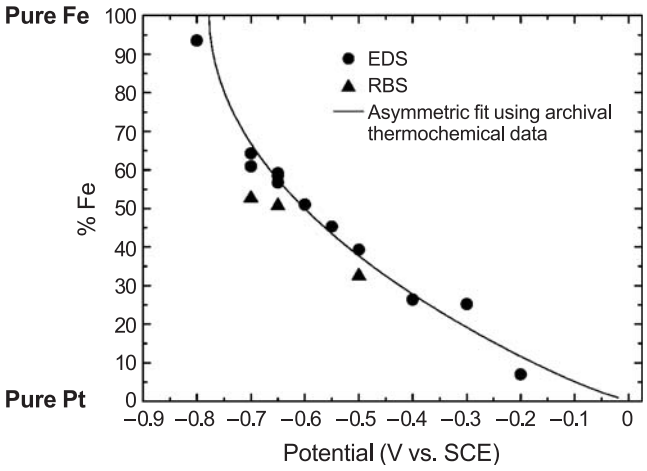

Figure 3: *The theoretical and experimental dependence of composition on the applied potential.*

The alloy composition of 300 nm thick films deposited from this solution was found to depend mainly on the applied potential and to be insensitive to the concentration of the solution components. A thermodynamic regular solution model was used to describe the dependence of film composition on applied potential. The comparison of theory to experimental data can be seen in Figure 3.

The deposited films were found to be remarkably smooth, with RMS roughness values less than 5 nm for micron-thick deposits. This was surprising given the large platinum overpotential (supersaturation), which usually results in growth instabilities and consequent roughening.

The control of crystal orientation is an essential consideration for high-density recording applications. A transition in the recording industry is currently in progress to perpendicular media, in which the bits are magnetized perpendicular to the plane of the medium. Maximum advantage can be derived from $L1_0$ FePt as a perpendicular medium when it is correctly aligned with its magnetic easy-axis perpendicular to the substrate plane. A careful choice of substrate and annealing parameters is required to recrystallize the as-deposited random fcc alloy to appropriately oriented $L1_0$.

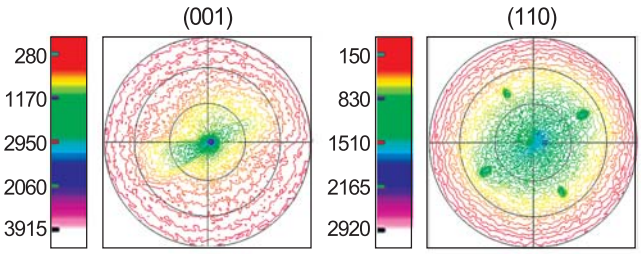

Figure 4: *X-ray pole figures showing favorably oriented FePt $L1_0$.*

FePt electrodeposited onto a Cu (001) substrate has recently shown great promise. X-ray diffraction revealed the transition to $L1_0$ upon annealing, and X-ray pole figures indicated favorable orientations. Figure 4 shows FePt $L1_0$ (001) and (110) pole figures. The (001) figure indicates perpendicular orientation of the magnetic easy-axis (the c-axis), while the (110) figure indicates an in-plane texture. The in-plane texture is an added advantage, as it results in a narrower switching field distribution.

Copper additions to the alloy have been found to lower the $A1/L1_0$ phase transition temperature by up to 90 ºC. It may be speculated that interdiffusion of copper from the substrate during the anneal allowed the recrystallization to proceed from the interface with the substrate. It is likely that this would allow the film to replicate the orientation of the substrate.

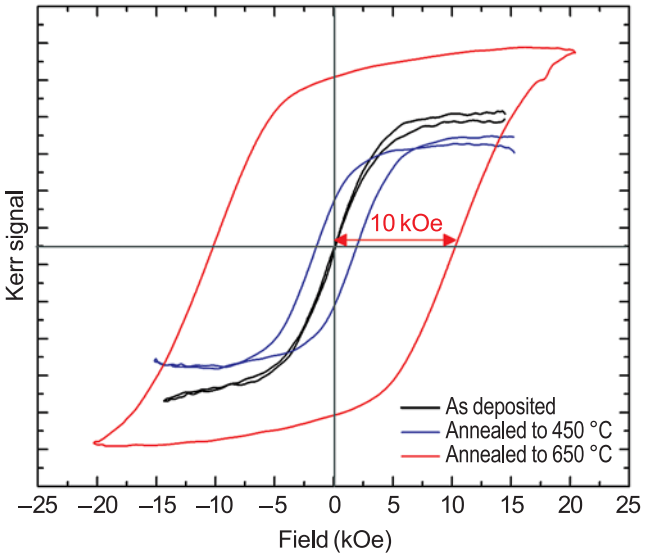

Figure 5: *Magnetic hysteresis measurements showing a 10 kOe coercivity.*

Magnetic hysteresis measurements performed using a Kerr magnetometer are shown in Figure 5. The magnetic coercivity of 10 kOe is comparable to figures quoted in the literature for vacuum-deposited FePt. It is believed to be the highest value reported for an electrodeposited film.

Current efforts focus on controlling the interdiffusion between substrate and film to minimize loss of magnetization in the alloy, and on moving from planar films to through-mask deposited arrays of FePt pillars.

For More Information on this Topic

W.F. Egelhoff, Jr. (Metallurgy Division, NIST); E.B. Svedberg (Seagate Research, Pittsburgh)

On-Chip Interconnects: Extending Performance of Sub-100 nm Lines

Conductors in on-chip metallizations are now reaching dimensions so small that defective seed layers are impacting manufacturing yields, and electron scattering on surfaces and grain boundaries is reducing electrical transport in the buried wires. Our goal is to provide tools to overcome these barriers. Recent efforts have quantified sources of the increased resistivity in wires made of silver, the most conductive of all metals, demonstrated seedless processing routes for copper wires, and improved understanding and modeling of the superfill fabrication process.

Daniel Josell and Thomas P. Moffat

The steady reduction of transistor dimensions in integrated circuits has been accompanied by similar size reductions of the on-chip interconnects that carry electrical signals, pushing the industrial technology for copper seed deposition close to its limit for defect-free sidewall coverage. Defects in seed layers, which arise from limitations in existing sputter technology, lead to voiding during electrodeposition of the copper metallization.

Additionally, with the dimensions of the copper wires in these metallizations now approaching the intrinsic mean-free-path length of the conduction electrons, scattering on the wire surfaces has begun to significantly reduce electron transport and, thus, the associated electrical conductance of the wires. With grains in these conductors similarly sized, a reduction is also to be expected from grain boundary scattering. While the penalty for both effects is increased power dissipation and reduced clock speed, the appropriate approach for mitigation requires quantitative determination of the relative sizes of the contributions.

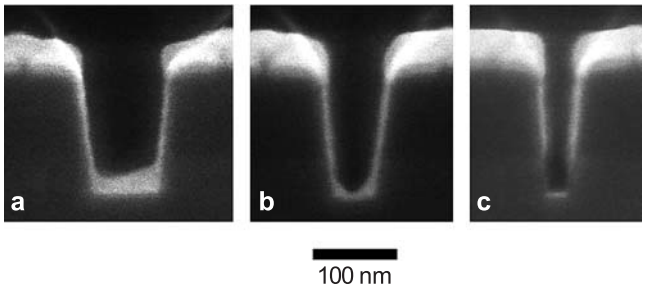

Figure 1: Ti/Pd/Ag seed layer in sub-100 nm deep trenches.

Technical Details

A tri-layer titanium, palladium and silver seed (Figure 1) was shown to yield smooth, conductive surfaces for the electrodeposition of silver wires for the electrical properties study. The poor seed coverage that is visible toward the bottom of the smallest trench (Figure 1c) is a technical challenge noted in the *International Technology Roadmap for Semiconductors*. Such seed defects motivated the "seedless" ruthenium barrier-based process detailed in last year's report and continued by this year's demonstration of seedless copper superfill in trenches with ruthenium or iridium barriers (Figure 2) deposited by perfectly conformal atomic layer deposition (ALD).

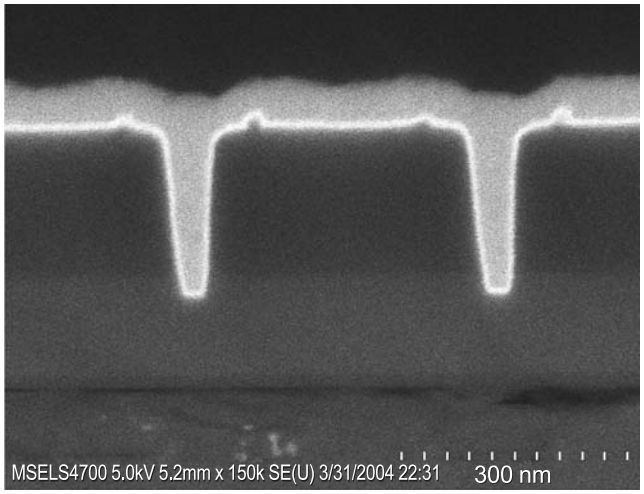

Figure 2: *Trenches containing copper that was electrodeposited directly on an ALD iridium barrier (thin bright layer).*

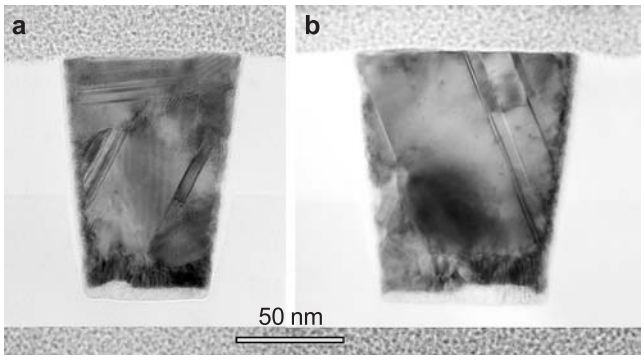

Figure 3: *Cross-section views of silver wires fabricated by electrodeposition in the seeded trenches followed by removal of the metal from the field (transmission electron microscope).*

For the electrical studies, silver wires (Figure 3) were fabricated by silver electrodeposition on the tri-layer seeds (Figure 1), using a superfill process developed in the Metallurgy Division, followed by removal of the metal in the field adjacent to the wires through chemical–mechanical planarization and ion polishing.

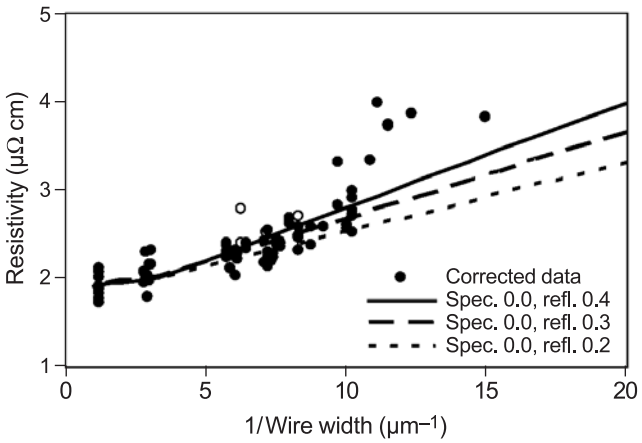

Figure 4: *Electrical resistivities of 300 nm tall silver wires compared to predictions that account for surface scattering with varying amounts of grain boundary scattering. Resistivities for wires less than 100 nm wide are impacted by defects.*

The wires were studied in a standard four-point probe geometry that permitted measurement of wire resistances. Resistivities, obtained from the resistances using measured wire dimensions, increased significantly with decreasing wire width (Figure 4). To assess the origin of the resistivity increase, the Fuchs–Sondheimer analysis for diffuse scattering of electrons on surfaces was extended to permit analysis in the presence of both specular and diffuse scattering. The resulting equations, along with a previously published equation for grain boundary scattering, permitted quantitative evaluation of the experimental data. Significantly, modeling of the data showed that the increase of resistivity with decrease of wire size arises as much from scattering on grain boundaries as from scattering on the wire surfaces. This indicates that efforts to mitigate size effects must increase grain size as well as surface specularity if they expect to be more than modestly successful.

The continuing industrial need for predictive simulation of feature filling spurred experiment and modeling of the superfill process itself. Consumption of adsorbed accelerator, a detrimental deviation from the surface segregation behavior that is responsible for the superfill process, was measured. Inclusion of such consumption in our Curvature Enhanced Accelerator Coverage (CEAC) model and computer code have made the filling predictions even more accurate.

This research has continued to impact industry, indicated by requests for our superfill code from Intel, Applied Materials, ST Microelectronics, and ATMI; an invited article on superfill in the *IBM Journal of Research and Development*; and invited presentations given at Cookson–Enthone, in addition to publications and presentations at conferences.

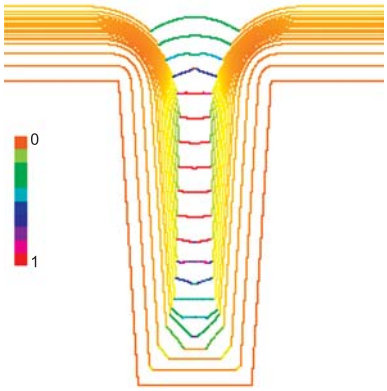

Figure 5: *Simulations of superconformal feature filling now account for consumption (incorporation) of adsorbed catalyst.*

Selected Project Publications for FY2004

T.P. Moffat, D. Wheeler, M. Edelstein and D. Josell, "Superconformal Film Growth: Mechanism and Quantification," *IBM J. Res. and Dev.,* in press.

D. Josell, C. Burkhard, Y. Li, Y.-W. Cheng, R.R. Keller, C.A. Witt, D. Kelley, J.E. Bonevich, B.C. Baker, T.P. Moffat, "Electrical Properties of Superfilled Sub-Micrometer Silver Metallizations," *J. Appl. Phys.* **96** (1), 759–768, (2004).

D. Wheeler, T.P. Moffat, G.B. McFadden, S. Coriell and D. Josell, "Influence of Catalytic Surfactant on Roughness Evolution During Film Growth," *J. Electrochem. Soc*. **151** (8), C538–C544, (2004).

T.P. Moffat, D. Wheeler, and D. Josell, "Electrodeposition of Copper in the SPS-PEG-Cl Additive System: I. Kinetic Measurements: Influence of SPS," *J. Electrochem. Soc.* **151** (4), C262–C271, (2004).

W.J. Evans, D.G. Giarikos, D. Josell, and J.W. Ziller, "Synthesis and Structure of Polymeric Networks of Silver Hexafluoroacetylacetonate Complexes of THF, Toluene, and Vinyltrimethylsilane," *Inorg. Chem.* **42**, 8255–8261, (2003).

For More Information on this Topic

D. Josell, T.P. Moffat (Metallurgy Division, NIST); G. McFadden (Mathematical and Computational Sciences Division, NIST); R.R. Keller, Y.-W. Cheng (Materials Reliability Division, NIST); C. Witt (Cookson–Enthone); C. Burkhard, Y. Li (Clarkson University); D. Wheeler (University of Maryland); T.K. Aaltonen, M. Ritala, M. Leskelä (University of Helsinki, Finland)

Particle Metrology and Nanoassembly

As technology migrates toward smaller physical dimensions, new analytical approaches are required to characterize material properties and to investigate critical issues. Our primary focus is the application of metrology and the development of new methods and standards for measuring the physical and surface properties of nanostructured particle systems. Applications include functional materials and devices for catalysis, power generation, and microelectronic, pharmaceutical, and biotechnology industries.

Vince Hackley

Nanocrystalline oxides of alkaline-earth cations produced by a supercritical drying process exhibit unique and highly reactive surface chemistries. As a result, these materials have been studied extensively as destructive adsorbents, catalysts, and bioactive agents. Investigations were concluded regarding the role of cation size on the evolution of microstructure in these materials and on the dispersion properties in aqueous NaCl solution. A series of small-angle neutron scattering (SANS) experiments were performed at the NIST reactor in collaboration with researchers at Kansas State University. These results indicate a complex picture for structure formation during the drying and annealing processes, with string-like gel morphology giving way to fractally rough particulate assemblies of compacted nanocrystals.

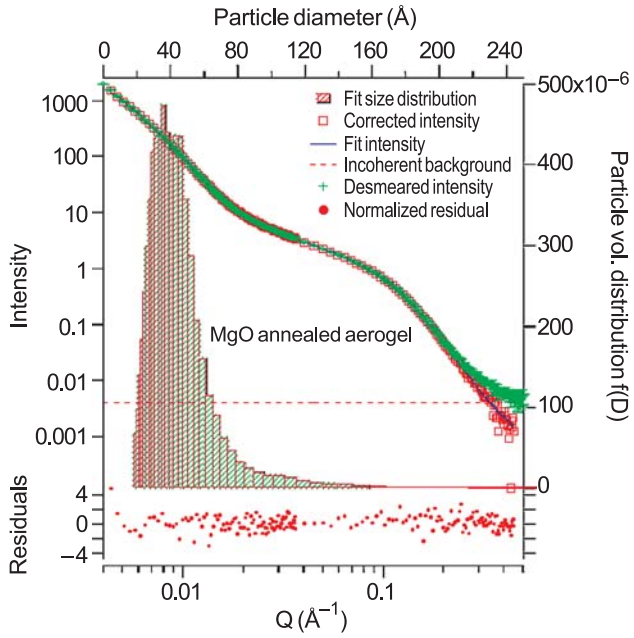

Figure 1: *Maximum entropy fit to SANS data for annealed MgO aerogel.*

Data were analyzed using the Unified Model of Beaucage and the maximum entropy method (see Figure 1). The scale of the finest structural features increases with increasing cation size for the annealed product. Analysis indicates the absence of mass fractal structures but the presence of surface fractal-like objects. A broad correlation peak in the data for heat-treated Mg and Ca oxides gives evidence for some local ordering of the nanocrystals. This data will help provide a more complete understanding of the structural development in this complex and technologically important system.

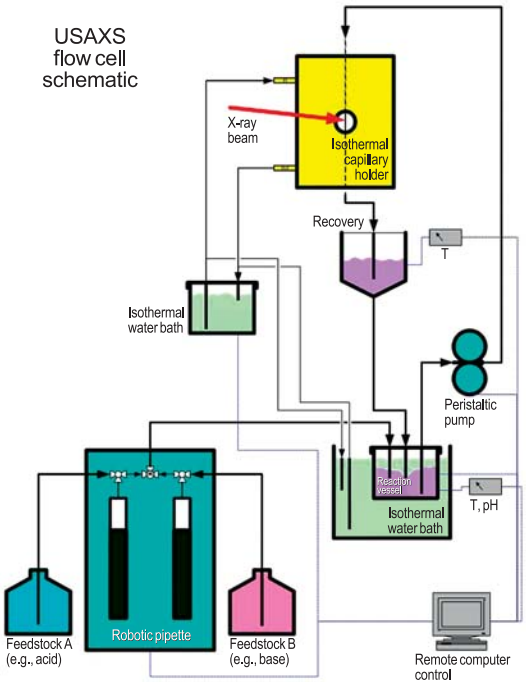

Figure 2: *Schematic diagram of capillary flow cell.*

A capillary flow-cell (Figure 2) was developed and commissioned for the ultra-small-angle x-ray scattering (USAXS) instrument on the UNICAT beam line at the Advanced Photon Source. This new capability will permit *in situ* investigations of complex multiphase particulate systems under controlled flow conditions. Initial applications include the dispersion of single-wall carbon nanotubes in collaboration with Rice University and depletion effects in binary colloidal suspensions.

Contributors and Collaborators

A. Allen, L. Lum (Ceramics Division, NIST); D. Ho (NIST Center for Neutron Research); K. Klabunde (Kansas State University); M. Pasquali (Rice University); P. Jemian (University of Illinois)

Nanostructure Fabrication Processes: Patterned Electrodeposition by Surfactant-Mediated Growth

Novel structures and devices can be formed through template electrodeposition. The ultimate pattern resolution is determined by the size and packing of molecules that comprise the template and their ability to inhibit or catalyze various electrochemical reactions. In the past year, the effect of molecular functionality on the metal deposition process has been explored.

Thomas P. Moffat and Michael J. Fasolka

Over the last decade, electrochemical processing has been undergoing a renaissance with the fabrication of new materials and novel microstructures. The development of new measurement techniques and metrological tools for studying controlled growth at fine length scales is the primary objective of this effort.

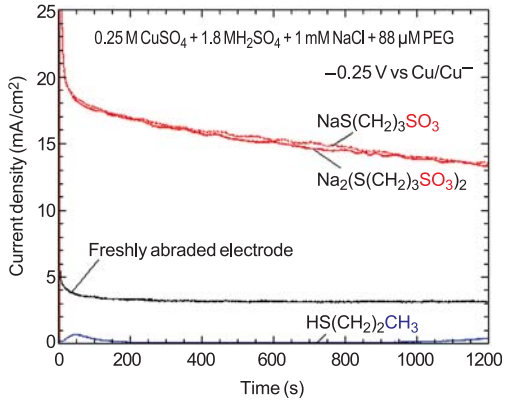

Figure 1: *Influence of small changes in molecular structure, i.e., SO_3^- vs. CH_3, on the rate of copper deposition.*

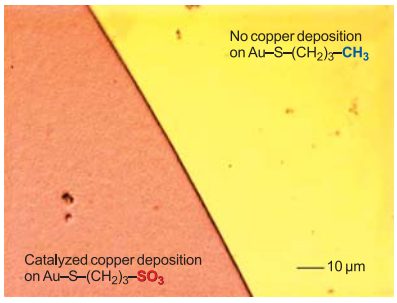

Figure 2: *Copper deposition on an alknethiol derivatized gold substrate only occurs in regions bearing $–SO_3^-$ terminated molecules.*

The three key metrology issues addressed are:

1. The rate differentiation accessible via surfactant mediated metal film growth;
2. The role of molecular functionality of the surfactant and robust design rules; and
3. The anisotropy induced in the electrocrystallization reaction rate for a given surfactant.

As an example, an alkanethiol monolayer film can either block or accelerate metal deposition depending on the molecular functionality of its terminal group. A dynamic range spanning several orders of magnitude is possible depending on the system in question (Figures 1 and 2). Based on these measurements, selective metal deposition may be obtained by patterning a substrate with the appropriate molecule.

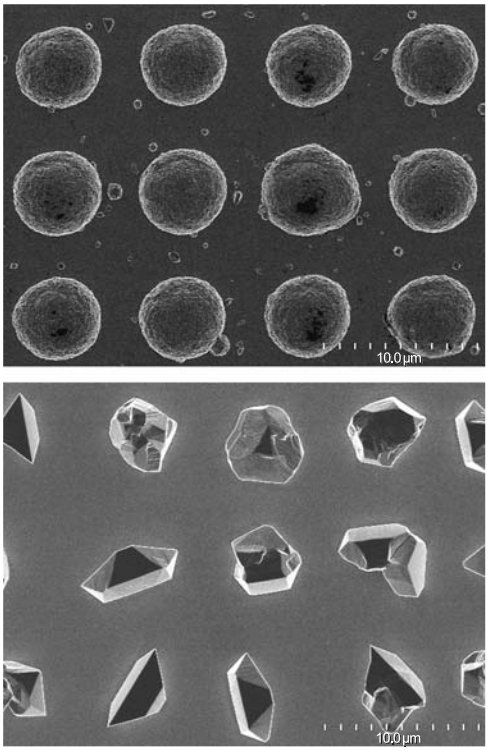

Figure 3: *Spatially patterned monolayer films used to control nucleation and anisotropic growth of copper crystals.*

Through contact printing, higher resolution patterning is possible, along with some interesting opportunities for high-throughput combinatorial research. By varying the surface chemistry, growth of isotropic or faceted crystals has been shown to be possible (Figure 3).

Contributors and Collaborators

D. Josell, J. Mallett, W.F. Egelhoff (Metallurgy Division, NIST); M. Walker, L. Richter (CSTL, NIST)

Nanostructure Fabrication Processes: Thin Film Stress Measurements

The microelectronics community uses electrodeposition to produce solderable surface finishes, magnetic recording media, and copper interconnections in printed circuit boards and integrated circuits. These films tend to develop sizable mechanical stresses that can lead to loss of adhesion and the generation of bulk and surface defects. This project focuses on the measurement of these stresses which should enable the development of effective mitigation strategies.

Gery R. Stafford and Ole Kongstein

Electrodeposited films tend to develop sizable mechanical stresses during deposition due to the nucleation and growth process or solution additives and alloying elements. We have established an optical bench dedicated to the *in situ* measurement of growth and residual stress during electrodeposition using the wafer curvature method. In one approach, a substrate of borosilicate glass is evaporated with 250 nm of gold. The force exerted on the cantilever by the electrodeposit causes curvature of the cantilever, which is monitored during electrodeposition. Forces on the order of 0.03 N/m can be resolved during film deposition.

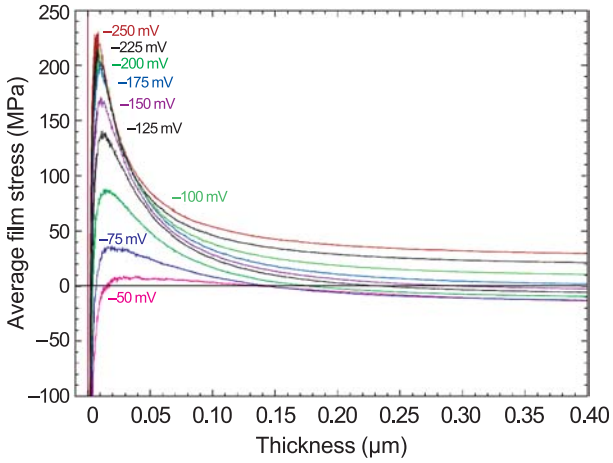

Figure 1: *Average film stress during copper deposition.*

Figure 1 shows the average in-plane stress associated with the deposition of copper from an additive-free sulfate electrolyte. The rapid rise in tensile stress (within the first 20 nm) and its dependence on deposition potential are consistent with nuclei coalescence and grain boundary formation. The highest tensile stresses are associated with high nucleation densities which are obtained at more negative deposition potentials. As the deposit thickens, the average film stress decreases and becomes compressive in deposits formed at small deposition overpotentials. In the physical vapor deposition literature, this compressive stress has been attributed to the non-equilibrium concentration of mobile ad-atoms on the surface that are driven into the grain boundaries.

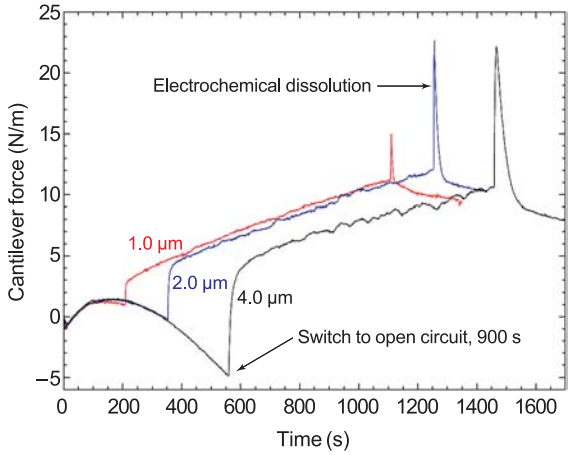

Figure 2: *Force/width exerted on the cantilever during the electrochemical processing of Sn on Cu.*

We have also examined the force exerted onto a copper cantilever electrode during the deposition of matte tin (Sn), Figure 2. This is a particularly important system since the growth of tin whiskers, known to produce electrical short circuits and device failure, has been attributed to both the residual stress in the electrodeposit as well as that generated from intermetallic formation at the Sn-Cu interface. The force curves show the following features: a tensile to compressive transition during deposition, a significant tensile relaxation when plating is discontinued, the development of tensile stress while the deposit is at open circuit, and a residual tensile stress after the deposit is electrochemically dissolved. The two latter features are attributed to the formation of the Cu_6Sn_5 intermetallic (IMC) at the Sn-Cu interface. A tensile stress is generated since the IMC has approximately 6 % smaller volume than a rule of mixture combination of the Sn and Cu reactants. Calculating the IMC thickness from the difference in Sn deposited and stripped, a nominal stress in the intermetallic was estimated to be 1.2 GPa after only one hour. Future work will focus on determining to what degree this increases the compressive stress in the Sn electrodeposit.

Contributors and Collaborators

W. Boettinger, U. Bertocci (Metallurgy Division, NIST)

Wet Nanomanufacturing

Wet nanomanufacturing is the generation of novel nanostructures and the control of chemical reactions (and signals) ***in a fluid environment****; this requires effective techniques and efficient material measurements. Therefore, we aim to develop sophisticated fluid-handling devices for directing material assembly, controlling material transport, and measuring material properties.*

Steven D. Hudson

Flow control is essential for fluid measurement and manufacturing applications. The type and strength of flow are often crucial for producing the desired structure and properties when assembling advanced materials. Using recent advances in microfluidic technology, we have developed a miniature tool without moving parts that mimics the function of a four-roll mill, a rheological and processing instrument.[1] Several microchannels converge to the measurement zone, where micro-particle-image velocimetry was used to map the flow field. By adjusting the relative flow rates, the full range of planar linear flows could be produced. This includes simple shear, which is inaccessible in the four-roll mill.

Figure 1: *Carbon nanotube clusters suspended in the microfluidic trap in extensional flow in the horizontal direction. The cluster at right has fractured from the main one. Also, an individual tube that has broken from the cluster is visible at the far left (arrow). Individual tubes have also been trapped and examined in flow.*

Most importantly, this new device works as a trap, so that particles and other objects can be examined in flow. Using this and related devices, clusters of carbon nanotubes suspended in fluids have been examined (Figure 1). In addition, extension and alignment of individual wormlike micelles has been measured as a function of flow strength and duration.

To achieve certain flow characteristics for particular measurement applications, other microchannel geometries have been and are being developed. Specifically, a device for measuring cell and tissue viability, and mechanical response, is being assembled. Also, a new instrument system for measuring interfacial tension has been developed.

Although microchannels are effective for these important functions, reaching a smaller scale efficiently, requires a new approach. Miniaturization towards nanochannels is usually not practical, because it necessitates very high pressures. At these smaller scales, membranes mediated by pores (as found in living systems) are likely to be efficient means to control the transport of material in metrological and nanomanufacturing processes.

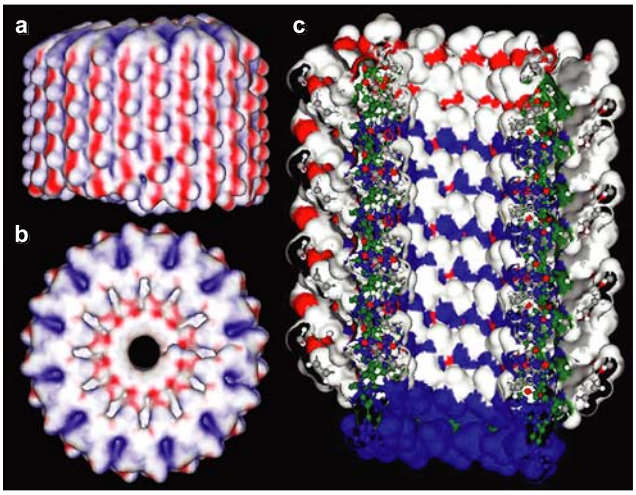

Figure 2: *Molecular model of the artificial membrane pore viewed from: a) the side, b) top, and c) in cross section.*

One such membrane pore (Figure 2) assembled by supramolecular chemistry has been characterized recently.[2] Determination of Fourier components (amplitude and phase) by transmission electron microscopy demonstrated that the supramolecular assemblies are tubular, with an inner diameter of 1.4 nm. Proton conduction through these channels has been measured to be comparable to the transmembrane protein channel gramacidin. Directed assembly of other artificial transmembrane channels will be explored.

References

1. Hudson, *et al.*, *Applied Physics Letters* **85**, (2004).
2. Percec, *et al.*, *Nature*, in press (2004).

Contributors and Collaborators

F. Phelan Jr., K. Migler, P. Start, P. Stone, J. Taboas, E. Hobbie, E. Amis, J. Cabral, K. Beers, J. Douglas, J. Pathak (Polymers Division, NIST); J. Kasianowicz (Biotechnology Division, NIST); V. Percec, D. Discher (University of Pennsylvania); R. Tuan (NIH)

Second Joint Workshop on Measurement Issues in Single-Wall Carbon Nanotubes: Purity and Dispersion, Part II

The 2nd Joint Workshop on Measurement Issues in Single-Wall Carbon Nanotubes, organized by the National Aeronautics and Space Administration, Lyndon B. Johnson Space Center (NASA-JSC) and the National Institute of Standards and Technology (NIST), was held January 26–28, 2005, at NIST in Gaithersburg, MD. In attendance were over 80 participants, representing private corporations, universities, and government laboratories. The primary purpose of the workshop was to bring together technical and business leaders in the field of single-wall carbon nanotubes (SWCNTs) to discuss measurement priorities and aid in the development of measurement protocols. The primary output of the meeting will be "NIST Recommended Practice Guides," authored by workshop participants and edited and published by NIST, for use by scientists and engineers involved in R&D, processing, and the production of nanotube containing products. These "Practice Guides" will contain measurement protocols that will help harmonize sample preparation, measurement procedures, data analysis, and reporting among the nanotube manufacturers, researchers and end users.

It was decided to revisit the topics of purity and dispersion, which were the subjects of the first NASA/NIST workshop held in May 2003. While progress in these measurements has been made, improvements are still needed to accurately measure and describe the quality of nanotube-containing materials and the dispersion of nanotubes in liquids or polymers, both of which are considered crucial for the continued growth of applications incorporating SWCNTs. The organizers recognized that there remains considerable confusion and ambiguity regarding which techniques to use for a particular purpose and the relative accuracy which one should expect to achieve. Significant differences in both methodology and interpretation continue to exist from one measurement laboratory to another. For this reason, comparison and specification of the quality of SWCNT materials is extremely difficult, as noted in *Nature*, 16th Dec. 2004.

To address these challenges, the organizing committee invited 23 speakers and developed an agenda that encouraged active participation from attendees. Breakout sessions addressing both workshop topics were held to foster open discussion and to invite consensus regarding best techniques and measurement methods. A half-day open discussion led to a consensus on those measurements for which protocols were most urgently needed.

Presentations

There were two Keynote Presentations. The first was given by Dr. Robert Haddon, from the University of California at Riverside, who presented the latest findings regarding the use of Near IR Spectroscopy (NIR) as a primary means of assigning a quantitative value to the purity of a SWCNT-containing sample. Significant progress has been made in the use of this technique since it was discussed at the first workshop. There was general agreement that NIR may be a viable technique to quantify purity, but there are several questions remaining, including affects of tube diameter and type of processing.

The second Keynote Address was given by Mr. James Von Ehr, the founder and president of Zyvex Corporation, who focused on the potential commercial applications for carbon nanotubes in a number of different areas. He called attention to the need for measurement techniques that would lead to improved qualification procedures for nanotubes from a given supplier.

The remainder of the first day was devoted to a number of plenary presentations on the topic of purity measurement, followed by breakout sessions whose goal was to identify the critical measurement issues relative to the determination of nanotube purity. A poster session with 25 posters was held in the evening to allow workshop participants to present their latest findings and to hold informal discussions with their colleagues.

The primary topic on the second day of the workshop was the measurement of nanotube dispersion. There were also several presentations on the characterization of isolated nanotubes. The end of the second day consisted of breakout sessions devoted to dispersion measurements.

The following sections provide some details of the important issues relative to measurement of purity and dispersion as discussed during the meeting.

Purity

The purity of single-wall carbon nanotubes was loosely defined by the attendees at the first workshop as the quantity of SWCNTs relative to other carbon-like materials present (amorphous, graphitic, and C_{60} carbons) as well as metal impurities. The point was made however that not all producers or users employed this definition in a way that allows for a quantitative assessment of the quality of a sample. A number of measurement techniques used for purity determination were discussed with the general consensus that no single technique can describe the quality of a sample

of nanotubes. After much discussion it was agreed that the most extensively utilized techniques are thermogravimetric analysis (TGA), scanning electron microscopy (SEM), transmission electron microscopy (TEM), Raman spectroscopy, and near infrared spectroscopy. The need for rapid, inexpensive measurement methods was emphasized.

Both TEM and SEM are used extensively for qualitative analysis of a sample containing SWCNTs. There was general accord that a TEM image demonstrating the existence of a significant quantity of SWCNTs is an important measure of the quality of the material. For quantitative estimation, a combination of TGA, Raman, NIR, and ICP methods was recommended.

Dispersion

Dispersion was divided into two categories, **macrodispersion**, defined as the distribution of nanotube bundles, and **nanodispersion**, the splitting of the bundles into individual tubes. In macrodispersion the primary issue is the agglomeration of SWCNTs in solvents or polymers, while in nanodispersion the focus is on eliminating SWCNT ropes. The question of dispersion stability over time was also viewed as important.

It was agreed that it is critical to have a consistent sample preparation for all the dispersion characterization methods. The technique of choice to determine the degree of macrodispersion appears to be optical microscopy. However, there is lack of agreement on what constitutes good *versus* poor dispersion. It was suggested that Raman mapping techniques, SEM, and scanned probe microscopy (SPM) may be useful complements to optical microscopy. Small angle scattering (neutron and X-ray) was put forward as a possible fundamental method to quantify dispersion.

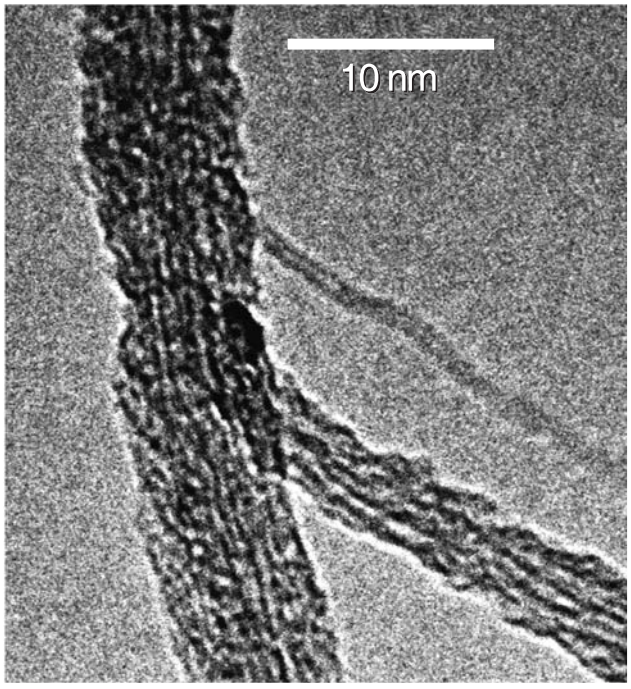

Figure 1: *TEM image of a SWCNT rope observed at NIST. The presence of impurities, mixtures of single and multi-walled nanotubes, defects, and tube bundling, coupled with the ultra-small dimensions, continue to complicate the characterization of these unique materials.*

Conclusions

The final session of the workshop was devoted to presentations of the synopses of each of the breakout sessions on the topics of purity and dispersion, and a general discussion and debate regarding priority needs for measurements. There was consensus that protocols for measurement techniques would be valuable even if they are incomplete.

On the topic of purity, the strengths, limitations, and research needs for a number of measurement techniques were discussed. A matrix showing techniques on one axis and the item measured on the other axis was used to reach a consensus for the most critical techniques to be addressed in the "Practice Guide." It was eventually agreed that chapters would be written on four primary procedures, TGA, TEM/SEM/SPM, Raman spectroscopy, and NIR, and two secondary techniques, inductively coupled plasma (ICP) and x-ray fluorescence. Volunteer authors were found for each of the chapters.

The attendees agreed that the topic of dispersion needed a separate "Practice Guide" from that of purity. The chapters for this "Practice Guide" were divided into the topics of macro- and nano-dispersion, and authors were found to write them. There was also a general agreement that one of the needs was an agreed upon terminology, which will be included in the "Practice Guide." The chapter on macrodispersion would be primarily devoted to microscopy procedures, while that on nanodispersion would include mention of a wide variety of techniques including small-angle-neutron and x-ray scattering, atomic force microscopy, etc.

A discussion was held regarding the need for reference materials. While there was consensus that such materials would be useful, it was felt that production of such materials should be delayed until the protocols for the measurement procedures are more firmly established. A number of participants also commented that inter-laboratory tests could be quite useful in establishing laboratory-to-laboratory correlations on measurements.

Finally, the question was raised regarding the need for future workshops of this kind. There was a general sense that future workshops would be valuable, but there was not consensus on the particular topic. However, nanotube dimension measurements and determination of chirality both received strong support.

Extraordinary Transport Properties of Nanotube/Polymer Nanocomposites

There has been intense interest in composites of polymers and carbon nanotubes (CNT) because of the large transport property (conductivity, elasticity, viscosity, thermal conductivity) changes exhibited by these additives for relative low CNT concentrations (≈ 1 % volume fraction). NIST's experience in the area of dielectric and rheological measurement, in conjunction with expertise in modeling, puts it in a unique position to lead the development of new processing concepts required by industry to utilize this important new class of materials.

Kalman B. Migler and Jack F. Douglas

The combination of extended shape, rigidity and deformability allows carbon nanotubes (CNT) to be mechanically dispersed in polymer matrices in the form of disordered network structures exhibiting a gel-like rheology. Our measurements on representative network-forming multi-wall carbon nanotube (MWNT) dispersions in polypropylene (PP) indicate that these materials exhibit extraordinary flow-induced property changes. Specifically, electrical conductivity σ and steady shear viscosity η both decrease strongly with increasing shear rate $\dot{\gamma}$, and these nanocomposites exhibit impressively large and *negative* normal stress differences, a rarely reported phenomenon in soft condensed matter. We illustrate the practical implications of these *non-linear* transport properties by showing that MWNTs *eliminate* die swell in our nanocomposites, an effect crucial for their processing.

The strong interest in CNT "nanocomposites" stems from their ability to affect thermal, electrical and rheological properties for relatively small concentrations of this type of additive. These additives have found manufacturing applications in electrostatic painting, protective coatings for electronic components, and flammability reduction. Utilization of CNT for more complex applications, however, requires an understanding of how processing conditions (mixing, molding, extrusion) influence nanocomposite properties.

Despite the high elastic modulus of CNT, their small cross-sectional dimensions and large aspect ratio allows them to bend substantially in response to inter-tube interactions under processing conditions. This bending leads to the formation of a disordered "web-like" structure (see Figure 1) of substantial mechanical integrity. The presence of a nanotube network interpenetrating

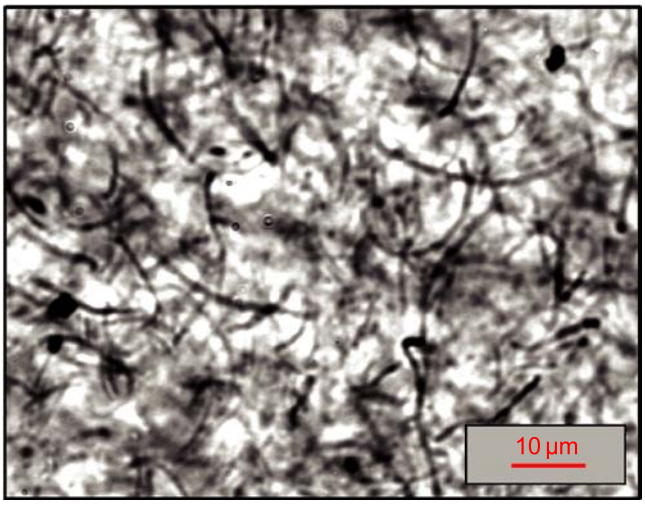

Figure 1: *Optical microscopy image of 1 % by volume MWNT/PP nanocomposite (obtained using a 100x objective) demonstrates good dispersion of the MWNT and reveals a polydispersity in nanotube length and shape. The MWNT volume fraction in this figure equals $\phi = 0.01$, which is close to the geometrical percolation concentration where the CNT network first forms and where the conductivity and stiffness of the nanocomposite increases by orders of magnitude (see Figure 2).*

the polymer matrix creates additional contributions to nanocomposite viscoelasticity that can have a radical effect on the processing characteristics of these materials.

In Figure 2, we characterize the large changes in viscoelasticity and conductivity for which polymer composites containing CNT are well known. *Simultaneous* measurements of σ and the shear moduli (G', G'') characterize the elastic and viscous properties of our composites. G' can be thought of as a measure of "stiffness" and G'' provides a measurement of viscous resistance to deformation. The ratio (G'/G'') or "loss tangent" ($\tan\delta$), is a measure of the composite "firmness," and we compare this basic quantity to σ. We observe that both (G'/G'') and σ increase with ϕ and that this variation becomes rapid for MWNT volume fraction ϕ in the range from 0.0025 to 0.01. We see that adding MWNT to the PP matrix increases the conductivity by an impressive seven orders of magnitude as a percolating network structure forms. G' and G'' become frequency independent as ϕ is varied through the "gelation concentration," $\phi_c \approx 0.01$.

In order to manufacture MWNT nanocomposites into usable shapes, we must understand how the network structure acts to influence their processing behavior. The linear rheological and electrical transport properties (Figure 2) are strongly altered by flow, as

Figure 3 indicates. Notably, both the conductivity and the viscosity $\eta(\dot{\gamma})$ exhibit a strong *thinning*. The viscosity decreases over the full range of shear explored here, whereas the conductivity shows a plateau region at low shear. Moreover, a positive normal force ΔN is observed in our nanocomposite for $\phi \leq \phi_c$, where the matrix dominates the rheological response (Figure 3), but ΔN becomes large and *negative* for $\phi \geq \phi_c$, compensating the large ΔN exhibited by the matrix polymer. (A negative ΔN in nanotube dispersions was reported by Lin–Gibson, *et al.*) This has significant processing consequences.

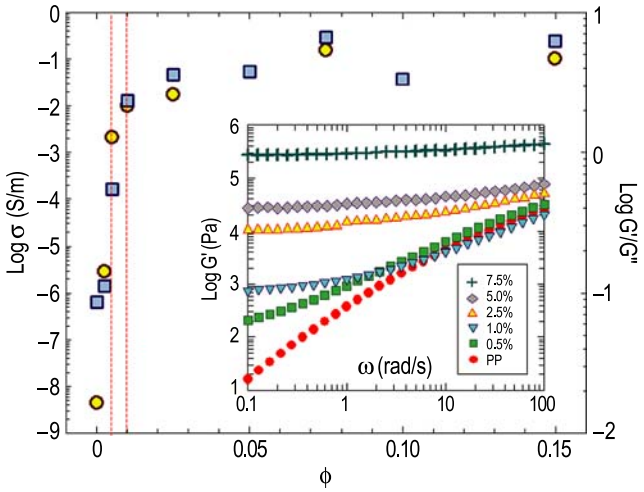

Figure 2: *Characterization of conductivity and viscolelasticity of MWNT/PP nanocomposites (ϕ = 0.025; T = 200 °C). Inset: Shear modulus as a function of frequency for a range of nanotube concentrations.*

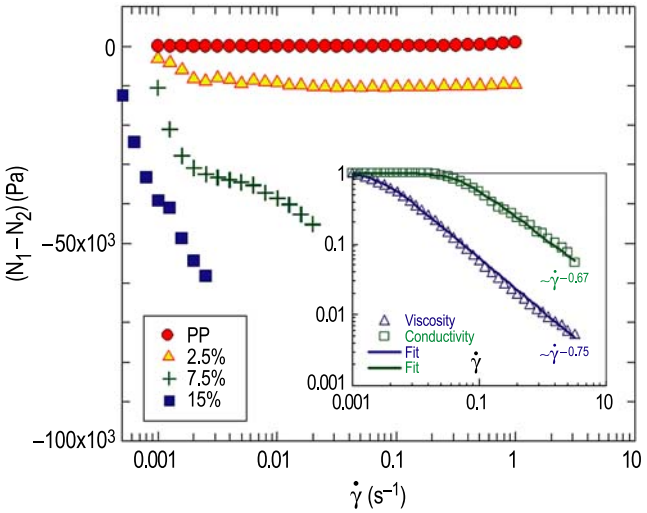

Figure 3: *Normal stress measurements showing slightly positive normal stress for pure PP and increasingly negative normal stress as the MWNT fraction increases. Inset: Conductivity and viscosity as a function of shear rate for (ϕ = 0.025; T = 200 °C).*

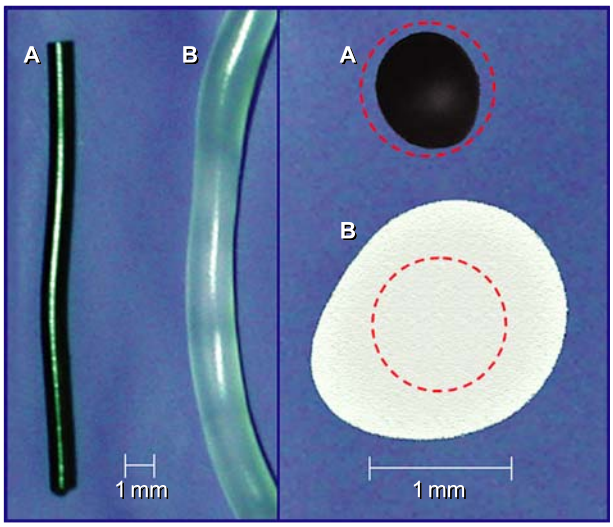

Figure 4: *Comparison of PP extrudate with (A) and without (B) added nanotubes. The red dashed lines correspond to the die size.*

Since the extrusion of the nanocomposite is a basic processing operation for which normal forces are known to be important, we extruded a nanocomposite sample (ϕ = 0.025) and found that the cross-section actually shrinks upon extrusion (Figure 4). This striking effect is contrasted with the extrusion of pure PP where a nearly 6-fold increase in cross-sectional area is observed. Evidently, the CNT change the qualitative nature of the polymer flow.

The suppression of die swell of extruded polymers by adding a relatively small amount of MWNT ($\phi \approx 0.01$) offers a powerful tool for controlling dimensional characteristics and surface distortion in manufacturing composites. Our observations of strongly non-linear rheology under flow (shear thinning and large, negative normal stresses) imply that these fluids should exhibit other "anomalous" flow characteristics (*e.g.*, droplet distortion and thread break-up) that are quite unlike Newtonian fluids. Understanding these flow characteristics is crucial for their processing.

For More Information on this Topic

S. Kharchenko, J. Obrzut, E. Hobbie (Polymers Division, NIST)

S. Lin–Gibson, J.A. Pathak, E.A. Grulke, H. Wang, and E.K. Hobbie, "Elastic Flow Instability in Nanotube Suspensions," *Physical Review Letters* **92**, 048302-(1-4) (2004).

S.B. Kharchenko, J.F. Douglas, J. Obrzut, E.A. Grulke, and K.B. Migler, "Extraordinary Flow Characteristics of Nanotube-Filled Polymer Materials," *Nature Materials*, in press.

Applications of Carbon Nanotubes: Carbon Nanotubes and Nanotube Contacts

A critical requirement for developing carbon nanotube based electronics is determining the mechanical and electrical characteristics of the connection between the carbon nanotube and its electrode. On this scale (nanometers), the properties of both the nanotube and the contact are not scaleable from larger measurements. To address this issue we are exploring a technique commonly used to manipulate the nanotubes and attach them to substrates inside the scanning electron microscope. We are subsequently developing the techniques to measure the small electrical currents and test the small mechanical strength associated with the contacts and nanotubes.

Paul Rice

We are developing techniques to measure the mechanical and electrical properties of carbon nanotube-based devices and also to image the nanometer-scale structure within the nanotube and their electrical contact. Shown in Figure 1 is a test device that we have fabricated to measure the electrical characteristics of an individual multiwalled carbon nanotube. The nanotube was attached, or welded, to the device in the scanning electron microscope (SEM) using an accepted technique called electron beam deposition (EBD). In this example, a single tube extends from one electrode to another.

Understanding the mechanical properties of the weld requires visualizing its structure on the atomic scale if possible. Using high-resolution microscopy techniques available within the division, we have seen some interesting new structures of the weld. Previously, it was assumed that the weld was a uniform material composed of amorphous carbon. However, we have seen, using atomic force microscopy (AFM) as well as transmission electron microscopy (TEM), spurious deposits of carbon far outside the weld. Figure 2 shows a nanotube welded to a chromium film. The residual carbon is seen as a surface texture that covers almost everything including the nanotube.

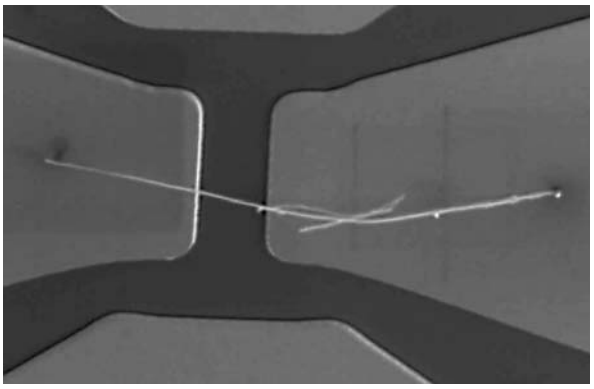

Figure 1: *SEM image of carbon nanotube test device for electrical measurements. The nanotube extends across a 2 μm gap. A second accidental tube is hanging on the side and is not connected to the electrodes.*

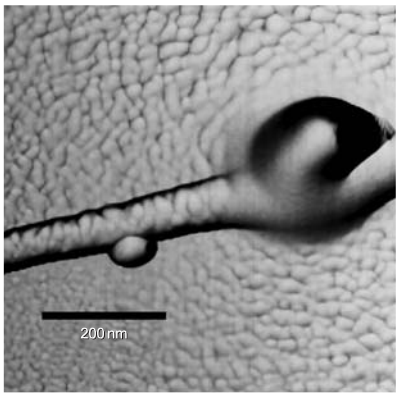

Figure 2: *AFM image of a multiwalled carbon nanotube welded to a chromium film. The orange peel texture is residual carbon left behind from the weld process.*

This work is beginning to shed some light on the properties and structure of these very small devices. A paper has been submitted entitled, "Electron Beam Deposition Welding: A Practical Application to Building Carbon Nanotube Devices," by P. Rice, R.H. Geiss, S.E. Russek, A. Hartman and D. Finch, to the *Journal of Vacuum Science and Technology* B. Further work is planned to measure contact resistance within the weld and resistance changes due to distortions caused by the weld process.

Demonstrating the need for better standards for nanotube device characterization, a new standards committee was recently formed by IEEE, on which NIST currently serves as a contributing member. Furthermore, presentations have been given to the American Vacuum Society, NASA Johnson Space Center, and the engineering department of the University of Colorado.

Contributors and Collaborators

R. Geiss (Materials Reliability Division, NIST); S.E. Russek, P. Kabos (EEEL, NIST); D. Finch, A.B. Hartman (University of Colorado)

Applications of Carbon Nanotubes: Cell Viability in Contact with Carbon Nanotubes

With the recent excitement about carbon nanotubes and their biological applications, preliminary studies are underway to determine the biocompatibility of nanotubes with cell cultures using our vascular smooth-muscle cell line. The response of these cells will help us understand the effects of cell proliferation or degradation due to direct contact with nanotube mats or clusters.

Paul Rice and Tammy Oreskovic

Carbon nanotubes (CNTs) have great potential for nanometer scale electronics, superior strength composites, biological implants, and many other applications where a well-organized nanometer scale material is needed. One possible application is using nanotubes as scaffold materials to support the growth of transplanted cells and establish proper orientation to grow artificial tissue. NASA has recently demonstrated growing retinal cells on nanotube mats. Other possible applications include sensors and probes for miniature biological devices, and electrodes for detecting biomolecules in solutions. However, many issues still remain in assessing the biocompatibility of these nanomaterial biosystems for *in vivo* applications.

In FY04, we explored the viability and proliferation of cells in contact with carbon nanotubes and dispersion techniques for compatible surfactants in cellular environments. In preliminary experiments, smooth muscle cells were exposed to both entangled mats and suspensions of multi-walled CNTs by use of surfactants for dispersion (Figure 1). Results of the proliferation assay indicate that there is a reduction in growth and metabolic activity for cells grown directly on the nanotubes as compared to the controls. These results indicate that cell attachment may not be as strong in regions of high CNT density. However, if the nanotubes are coated with a biologically compatible surfactant and suspended in media, there appears to be little effect when compared to the controls. Figure 2 shows preliminary results of an Alamar blue proliferation assay.

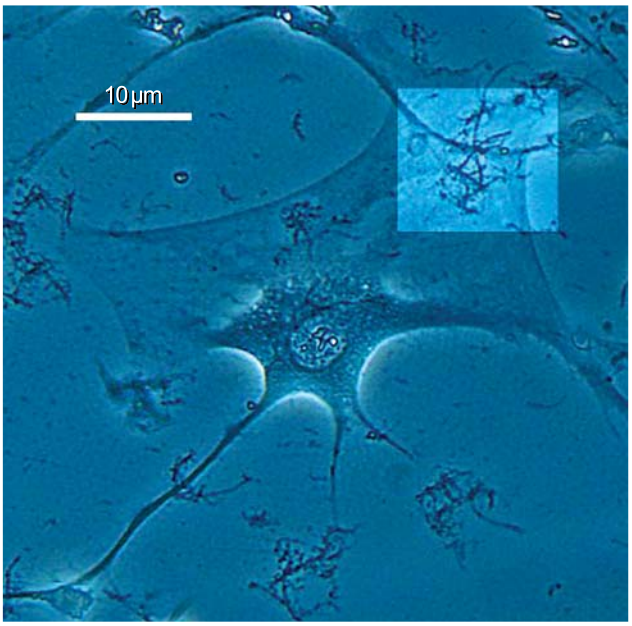

Figure 1: *Vascular smooth muscle cell growing on a cluster of multiwalled carbon nanotubes on a glass substrate.*

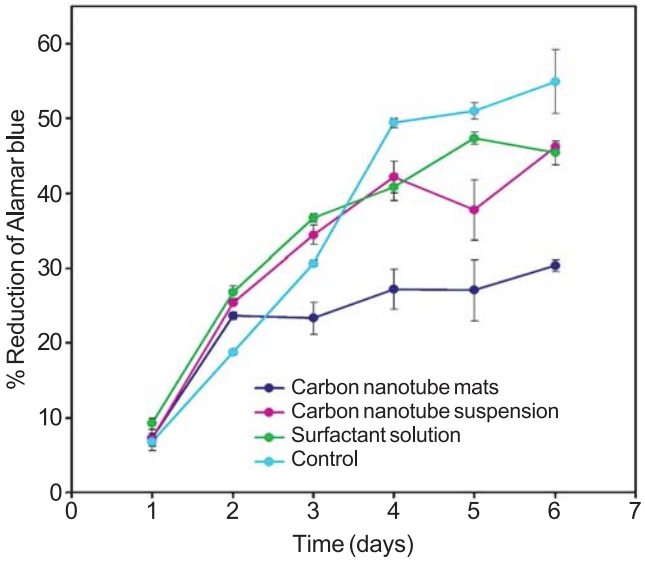

Figure 2: *Alamar blue assay, test for cell growth and proliferation. As the cells grow and divide they metabolize the Alamar blue compound, changing the medium in which the cells are growing from a blue color to clear.*

In FY05, we will continue to explore the interactions of structure and the effects of clumping of CNTs on cell growth and orientation. Other possible directions may include surface modification to promote cell adhesion and growth, tomography, and size distribution of CNTs.

Contributors and Collaborators

Dr. N. Varaksa contributed the work on the surfactant chemistry; Dr. E. Gruelky (University of Kentucky) supplied carbon nanotubes.

Applications of Carbon Nanotubes: Electrochemical Characterization of *In-Vivo* Neuronal Probes

Instruments for in-vivo *recording of neural activity are critical for ongoing and future research aimed at Alzheimer's, Parkinson's, epilepsy, stroke, and spinal cord injuries. In addition, the development of a human-brain-machine interface (HBMI) relies on improved recording and processing of neuronal signals. Future recording electrodes must be small, stable, biocompatible, and robust. More rugged test procedures are also needed for evaluating and qualifying new electrode materials.*

Stephanie A. Hooker and Dudley Finch

New tools are needed to better image and measure signal transfer inside live cells. One conventional approach to electrical measurements in cellular materials involves a two-electrode glass micropipette that clamps the cell membrane. The discovery of this device, referred to as a patch clamp, in 1972 had widespread impact, leading to a Nobel Prize in 1991. However, the patch clamp is too large for many of today's desired measurements in neurobiology, due to the extent of physical damage caused during its insertion and use.

Recently, silicon-based MEMS technology has been explored as a method to produce smaller probes for neuronal research. These devices typically consist of a silicon shank (several hundred micrometers long) with an array of microelectrode recording sites located along its surface. In this manner, multiple neurons can be studied simultaneously with a single insertion point.

While these devices show considerable promise, many biologists continue to employ individual metallic wires as their primary recording electrodes. These wires are similar to those used inside the patch clamps but are inserted directly into the brain. Polymer coatings are often applied to increase impedance, enable better handling, and improve biocompatibility. The wires are typically tungsten or stainless steel with diameters on the order of 50–100 microns. To date, few studies have attempted to optimize the wire material, the coating, or the insertion technique (applied force, speed, etc.).

In collaboration with the University of Colorado's Health Sciences Center and the Departments of Chemistry, Electrical Engineering, and Mechanical Engineering at the University of Colorado at Boulder, we are developing measurements to help improve and optimize *in-vivo* probes. In FY04, we completed preliminary studies of wires (25 µm in diameter) coated with thin (~60 nm) layers of aluminum oxide, Al_2O_3. Atomic layer deposition (ALD) was used to precisely control coating thickness, and seven different wires were compared to determine metal effects on performance.

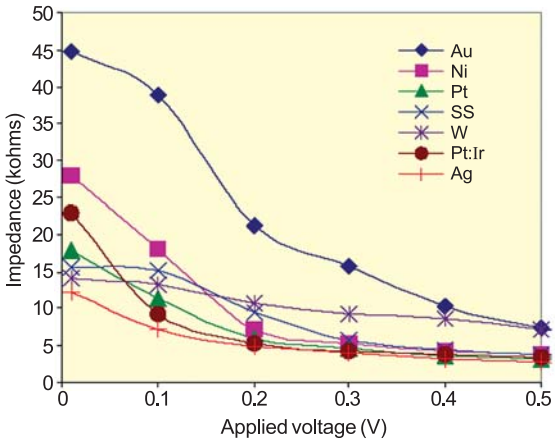

Figure 1: *Electrochemical impedance of ALD-coated microwires in Ringer's solution as a function of applied voltage at 100 Hz.*

A two-electrode configuration was used for testing in a Ringer's buffer solution. Several procedural variables were evaluated, including the type and size of the reference wire, the solution temperature and pH, and the electrode placement. Impedance was measured as a function of frequency, voltage (Figure 1), and time. The latter indicates the stability and reliability during extended recordings, a key requirement for long-term studies. Stability measurements will continue during the upcoming months in order to ensure that the ALD coating is not degraded either chemically (by the solution) or electrically (by the measurement itself).

However, it should be noted that 25 µm wires are still too large for subcellular studies. As a result, we plan to evaluate carbon nanotube (CNT) probes in FY05. CNT-based AFM probes have already been developed by other researchers in the Materials Reliability Division for studying microelectronic films. Moreover, dielectric coatings have recently been applied to individual tubes (via ALD) to further enhance signal transfer. If successful electrochemical measurements can be demonstrated, CNT based *in-vivo* probes could have a significant impact on neuroscience due to their small size (0.1 µm or less) and anticipated long-term stability.

Contributors and Collaborators

D. Restrepo, A. Sharp (University of Colorado Health Sciences Center); R. Artale, K. Gall, S. George, R. Zane (University of Colorado at Boulder)

Organizational Charts

Materials Science and Engineering Laboratory

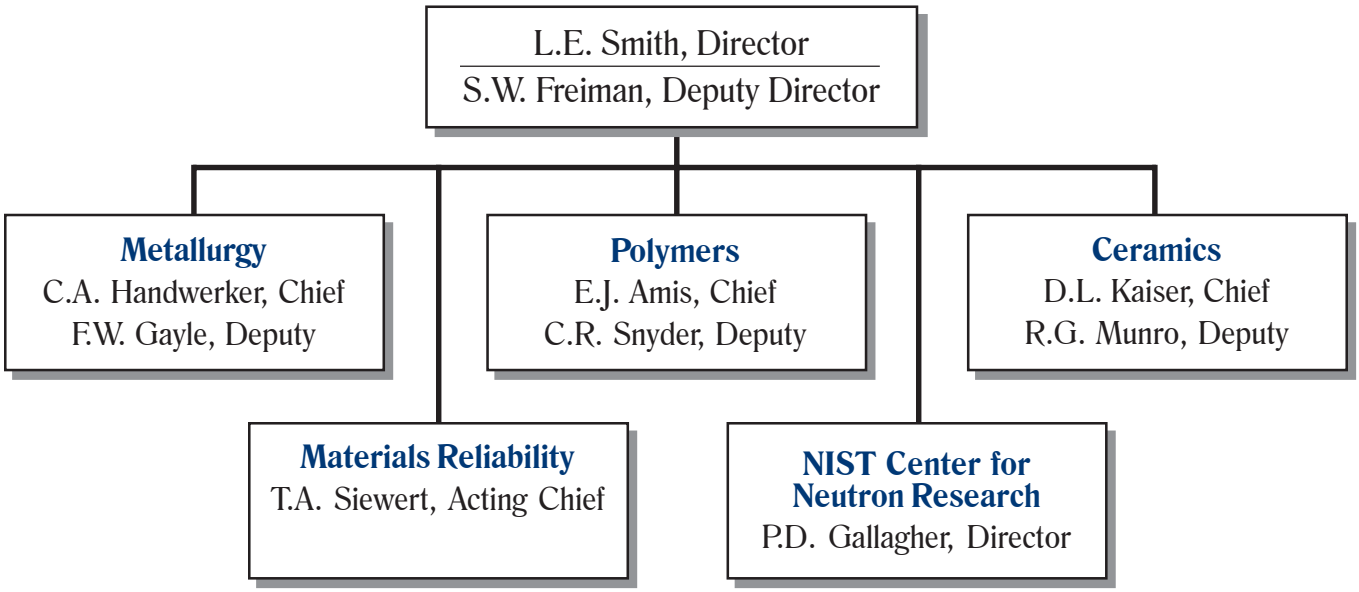

National Institute of Standards and Technology

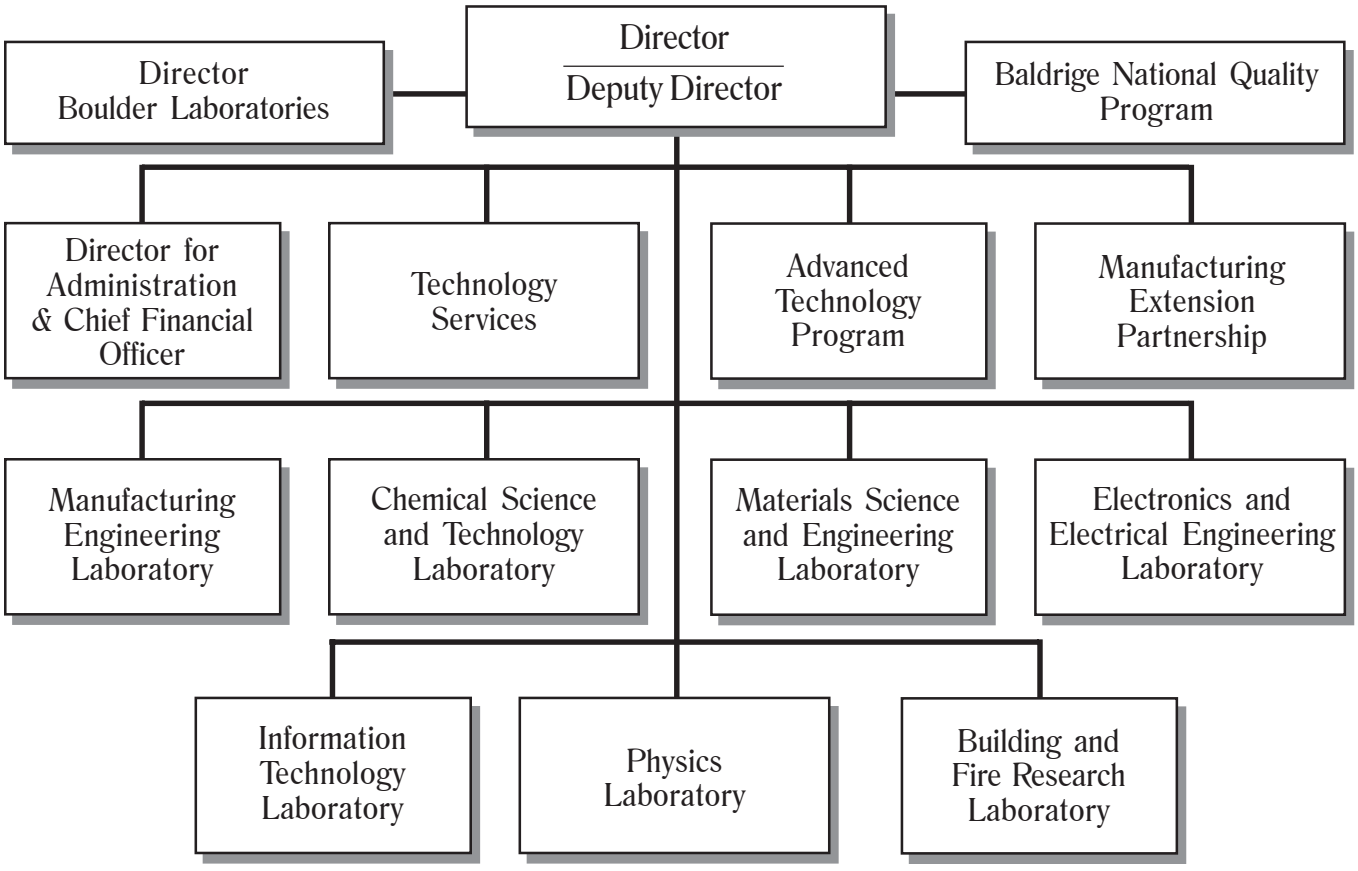

NIST